Basal ppGpp regulation by SpoT coordinates metabolic homeostasis and acid resistance

Yueyue Liu[1#], Muriel Leandra Schicketanz[1#^], Xichuan Zhai[2], Ling Deng[2], Kenn Gerdes[3], Yong Everett Zhang[1*]

[1] Department of Biology, University of Copenhagen, DK-2200 Copenhagen, Denmark

[2] Section of Food Microbiology, Gut Health, and Fermentation, Department of Food Science, University of Copenhagen, Rolighedsvej 26, 1958 Frederiksberg C, Denmark

[3] Independent Researcher, Copenhagen, Denmark

[#] Y.Y.L. and M.L.S. contributed equally to this work.

^ Current address: Novonesis A/S, Kgs. Lyngby, Denmark

*Correspondence: Yong Everett Zhang zhangy830328@gmail.com

Running title: Basal ppGpp links metabolism and acid resistance

Abstract

Bacteria survive fluctuating and hostile environments by coordinating core metabolism with stress-protective responses. How these processes are integrated at the molecular level remains incompletely understood. Here, we uncover a previously unrecognized role for the stringent response enzyme SpoT in coordinating amino acid homeostasis and acid resistance through maintenance of a basal pool of the alarmone ppGpp. Focusing on a conserved histidine residue in SpoT (H414), we show that its disruption causes severe growth defects in minimal medium and catastrophic acid sensitivity in *Escherichia coli*, independently of the canonical RelA-mediated stringent response. Transcriptomic and genetic analyses reveal that a SpoT H414A substitution leads to misallocation of metabolic flux, characterized by excessive arginine biosynthesis and concomitant depletion of intracellular glutamate, the essential substrate for the glutamate-dependent Gad acid resistance system. Intragenic suppressor mutations within *spoT* restore growth and acid resistance by re-establishing a sub-basal yet physiologically sufficient ppGpp pool, demonstrating that very low levels of ppGpp are required for metabolic balance and stress preparedness. Importantly, the requirement for SpoT H414 in supporting growth and acid survival is conserved in pathogenic *Salmonella* and *Shigella*. Together, our findings establish SpoT-derived basal ppGpp as a distinct regulatory regime that integrates metabolism and acid resistance, providing a framework for understanding how bacteria maintain physiological homeostasis and survive acidic environments.

KEYWORDS: basal ppGpp, SpoT, stringent response, metabolic homeostasis, acid resistance, Gad system

38 **Introduction**

39 Bacteria inhabit environments that fluctuate dramatically in nutrient availability and
40 physicochemical stress. To survive these challenges, cells must coordinate metabolic activity with
41 stress-protective responses in a manner that preserves essential resources while maintaining
42 viability. In enteric bacteria, exposure to acidic conditions, such as those encountered during
43 passage through the mammalian stomach, represents a particularly severe and ecologically relevant
44 challenge. Survival under these conditions is a key determinant of fitness and virulence[1], yet the
45 mechanisms that integrate metabolic state with acid resistance remain incompletely understood.

46 *Escherichia coli* exemplifies bacterial acid adaptation, surviving exposure to pH values as low as
47 2.5 through multiple acid resistance (AR) systems[2-4] Among these, the glutamate-dependent Gad
48 system provides the most robust protection under extreme acid stress by coupling proton
49 consumption to amino acid metabolism. Cytoplasmic glutamate decarboxylases (GadA and GadB)
50 convert glutamate to γ-aminobutyrate (GABA), consuming intracellular protons, while the GadC
51 antiporter exchanges GABA for extracellular glutamate to sustain the cycle[5,6]. This system is tightly
52 regulated[3,6] and energetically costly, requiring precise coordination between metabolic capacity,
53 substrate availability, and stress signalling. How cells ensure that sufficient glutamate is available to
54 support acid resistance under nutrient-limited conditions remains a central unresolved question.

55 Amino acid metabolism is globally regulated by the stringent response, a conserved bacterial
56 signaling network mediated by the alarmones guanosine tetra- and pentaphosphate (ppGpp)[7-10]. In
57 *E. coli*, the ribosome-associated enzyme RelA synthesizes large bursts of ppGpp in response to
58 amino acid starvation[11-15], triggering extensive transcriptional[16,17] and metabolic[18-21]
59 reprogramming. This acute stringent response represses stable RNA synthesis[16,17], remodels
60 nucleotide metabolism[18-21], and promotes amino acid biosynthesis[22-24], thereby restoring metabolic

61 balance during nutrient stress[25]. While the role of RelA-driven ppGpp accumulation has been
62 extensively characterized, the function of its paralog SpoT remains less well defined[7,26].

63 SpoT is unique among stringent response enzymes in possessing both ppGpp synthetase and
64 hydrolase activities[27,28] . In contrast to RelA, SpoT produces lower levels of ppGpp and responds to
65 a broader range of environmental cues, including fatty acid limitation[29,30], iron starvation[31], and
66 other non–amino acid stresses[32-36]. Genetic and physiological studies have implicated SpoT in
67 virulence, persistence, and stress adaptation across diverse bacterial species[7,33,37], yet its specific
68 regulatory role and downstream physiological functions remain poorly understood. In particular,
69 whether SpoT-derived ppGpp represents merely a weaker version of the canonical stringent
70 response or instead constitutes a distinct regulatory regime has remained an open question.

71 Here, we address this gap by dissecting the function of SpoT in the absence of RelA. We identify a
72 conserved histidine residue (H414) in the C-terminal regulatory region of SpoT that is essential for
73 maintaining a basal level of ppGpp. Mutagenesis of this residue to alanine uncouples amino acid
74 metabolism from acid resistance, leading to glutamate starvation, transcriptional collapse of the Gad
75 system, and extreme acid sensitivity. Through intragenic suppressor analysis, enzymatic
76 perturbations, and physiological rescue experiments, we demonstrate that a sub-basal yet non-zero
77 pool of ppGpp is both necessary and sufficient to coordinate metabolic homeostasis and acid
78 defense. Finally, we show that this SpoT-dependent regulatory logic is conserved in pathogenic
79 enterobacteria, underscoring its broader relevance to bacterial survival and virulence.

80 Together, our findings reveal SpoT-derived basal ppGpp as a central integrator of metabolism and
81 stress resistance, expanding the conceptual framework of the stringent response beyond RelA-
82 mediated acute starvation signaling to include a foundational role in bacterial physiological
83 homeostasis.

84 **Results**

85 **Mutagenesis of the conserved H414 residue of SpoT leads to defective growth in minimal**
86 **medium**

87 To investigate how SpoT integrates environmental cues independently of RelA, we focused on the
88 C-terminal regulatory region of SpoT, which is highly conserved among RelA/SpoT homologs but
89 poorly understood mechanistically. Sequence alignment revealed a conserved histidine residue
90 (H414 in *E. coli* SpoT) within the TGS domain, corresponding to H432 in RelA (**Extended Data**
91 **Fig. 1a, 1b**), a critical residue in sensing amino acid starvation[12-15].

92 To probe the functional role of this residue, we generated a SpoT H414A substitution in a *ΔrelA*
93 background. While the Δ*relA* $spoT^{wt}$ (hereto after $spoT^{wt}$) strain grew normally, the H414A mutant
94 ($spoT^{H414A}$) unexpectedly failed to grow on glucose minimal medium (M9Glc), both on solid and in
95 liquid culture (**Fig. 1a, 1b**). This severe growth defect was not anticipated and suggested a critical
96 role for SpoT H414 in supporting growth under nutrient-limited conditions. The unexpected growth
97 failure of $spoT^{H414A}$ cells prompted us to investigate the underlying molecular basis of this
98 phenotype.

99 **Transcriptomic analysis of $spoT^{H414A}$ cells reveals collapse of stress and acid resistance**
100 **programs**

101 To gain insight into the molecular defects underlying the growth failure of $spoT^{H414A}$ cells, we
102 performed transcriptomic analysis of the $spoT^{H414A}$ and $spoT^{wt}$ strains. Because $spoT^{H414A}$ cells
103 failed to proliferate in M9Glc, cultures were incubated under identical conditions until the $spoT^{wt}$
104 strain entered early exponential phase, at which point RNA was harvested from both strains
105 (**Extended Data Fig. 1c**).

106 Unexpectedly, RNA sequencing revealed extensive transcriptional dysregulation in *spoT*^{H414A} cells,
107 with strong repression of stress adaptation and acid resistance genes. Among the most prominently
108 downregulated loci were the glutamate-dependent Gad acid resistance system (*gadE*, *gadX*, *gadW*,
109 *gadA*, *gadB*, *gadC*), as well as additional components of the acid fitness island, including the
110 periplasmic chaperones *hdeAB* (**Fig. 2a, 2b**). Genes associated with osmotic and general stress
111 responses were similarly reduced; in contrast, genes linked to phage shock and SOS responses were
112 strongly induced (**Extended Data Fig. 1d-f**), suggesting widespread physiological stress. The
113 unexpected transcriptional collapse of acid resistance pathways prompted us to directly examine the
114 acid survival phenotypes of *spoT*^{H414A} cells.

115 **SpoT, but not RelA, is required for survival under extreme acid stress**

116 Guided by the pronounced transcriptional repression of acid resistance genes in *spoT*^{H414A} cells, we
117 next examined survival under lethal acid stress. Upon exposure to pH2.5, *spoT*^{H414A} cells exhibited
118 extreme acid sensitivity, with viability declining rapidly and no detectable survivors after 60
119 minutes (**Fig. 2c**). In contrast, both the parental wild-type strain and the *spoT*^{wt} strain survived acid
120 challenge efficiently, demonstrating that RelA is dispensable for acid resistance under these
121 conditions.

122 Notably, despite the severe acid sensitivity of *spoT*^{H414A} cells, viability under neutral, well-buffered
123 conditions (M9Glc) was preserved (**Extended Data Fig. 1g**), indicating that SpoT H414 is
124 specifically required for stress preparedness rather than basal viability. Together, these results
125 establish SpoT as the primary stringent response enzyme supporting acid survival in *E. coli*,
126 independently of RelA.

127 **Transcriptomic signatures indicate arginine metabolic overflow and glutamate depletion**

128 To define the metabolic basis of the growth defect observed in *spoT*^{H414A} cells, we examined
129 transcriptomic changes in central metabolic pathways. While expression of many amino acid
130 biosynthetic genes was modestly reduced, one pathway stood out: arginine biosynthesis was
131 strongly and coordinately upregulated (**Fig. 3a, 3b**). All the nine enzymes of the arginine
132 biosynthetic pathway exhibited significantly increased expression, together with *carAB*, which
133 supplies carbamoylphosphate to this pathway. This transcriptional pattern indicates a pronounced
134 redirection of metabolic flux toward arginine production.

135 In contrast, genes directing carbamoylphosphate toward pyrimidine nucleotide biosynthesis were
136 downregulated, suggesting selective diversion of this shared intermediate rather than a generalized
137 increase in anabolic metabolism. Because arginine biosynthesis consumes glutamate as a precursor,
138 the coordinated induction of the *arg* operons predicts substantial depletion of intracellular glutamate
139 pool.

140 In parallel with arginine pathway induction, genes involved in *de novo* purine nucleotide
141 biosynthesis were broadly upregulated (**Extended Data Fig. 2**). Many of these reactions consume
142 glutamine as a nitrogen donor, which is regenerated from glutamate, thereby imposing an additional
143 indirect drain on glutamate availability. Thus, simultaneous activation of arginine and purine
144 biosynthetic programs is predicted to exacerbate glutamate depletion, compounding the metabolic
145 imbalance caused by SpoT H414A mutation.

146 Together, these transcriptional signatures suggest that SpoT H414A leads to misallocation of
147 metabolic resources, with excessive flux into arginine biosynthesis and increased purine nucleotide
148 production collectively depleting glutamate. Given the central role of glutamate in both cellular
149 metabolism and acid resistance, this metabolic imbalance provides a unifying explanation for the

150 growth and stress survival defects observed in *spoT*^{H414A} cells and prompted us to directly test the
151 role of glutamate availability in these phenotypes.

152 **Glutamate starvation underlies the growth defect of *spoT*^{H414A} cells**

153 Prompted by the transcriptomic evidence for glutamate depletion, we tested whether exogenous
154 supplementation could restore growth. Addition of glutamate to M9Glc markedly improved growth
155 of *spoT*^{H414A} cells, substantially shortening the lag phase and increasing final biomass (**Fig. 3c**). In
156 contrast, supplementation with arginine or uracil failed to restore growth, and combining these
157 metabolites with glutamate provided no additional benefit.

158 Amond all 20 amino acids, supplementation with glutamine, asparagine, or proline partially
159 restored growth, consistent with their metabolic proximity to glutamate, but none matched the effect
160 of glutamate itself (**Extended Data Fig. 3a**). Increasing the concentration of glutamate up to
161 tenfold failed to further improve growth (**Extended Data Fig. 3b**), and combining glutamate with
162 glutamine, asparagine, or proline did not enhance regrowth beyond that achieved with glutamate
163 alone (**Extended Data Fig. 3c**). In contrast, supplementation with all 20 amino acids fully restored
164 the growth defect of *spoT*^{H414A} cells to a level exceeding that of the *spoT*^{wt} strain (**Extended Data**
165 **Fig. 3d**), indicating that glutamate starvation represents the dominant but not exclusive metabolic
166 limitation imposed by SpoT H414A dysfunction. Importantly, glutamate supplementation had only
167 minimal effects on the growth of a ppGpp^{0} (*ΔrelA ΔspoT*) strain (**Extended Data Fig. 3e**),
168 indicating that the rescue of *spoT*^{H414A} growth depends on residual SpoT activity rather than simple
169 nutritional supplementation.

170 To directly test whether arginine biosynthesis drives glutamate depletion, we deleted *argA*,
171 encoding the first committed enzyme of the arginine biosynthetic pathway. The resulting *spoT*^{H414A}

172 *ΔargA* strain failed to grow in M9Glc (**Fig. 3d**). Strikingly, arginine, but not glutamate, restored
173 growth in this background, demonstrating that blocking arginine synthesis prevents glutamate
174 depletion and alleviates the growth defect.

175 Conversely, artificial induction of arginine overflow phenocopied the *spoT*^{H414A} growth defect.
176 Overexpression of a feedback-resistant ArgA variant (ArgA^{H15Y})[38] delayed growth in M9Glc, and
177 this delay was significantly alleviated by glutamate supplementation (**Fig. 3e**). Together, these
178 results demonstrate that SpoT H414 prevents arginine-driven glutamate starvation, thereby
179 maintaining amino acid homeostasis required for growth in minimal medium.

180 **Basal SpoT activity supports glutamate-dependent acid resistance**

181 Because glutamate is the essential substrate for the Gad acid resistance system, we next asked
182 whether glutamate depletion contributes to the acid sensitivity of *spoT*^{H414A} cells. Supplementation
183 of the acid challenge medium with glutamate fully rescued survival during short-term acid exposure
184 and substantially improved long-term viability (**Fig. 4a**). In contrast, supplementation with arginine
185 or lysine provided only modest protection (**Extended Data Fig. 4a**), consistent with the dominant
186 role of the glutamate-dependent Gad system under extreme acid stress.

187 To determine whether impaired regulation of the Gad system accounted for the acid resistance
188 defect, we ectopically expressed *gadE*, the master transcriptional activator of Gad genes. Even low-
189 level expression of *gadE* significantly restored acid resistance in *spoT*^{H414A} cells, and combined
190 supplementation with glutamate further enhanced survival (**Extended Data Fig 4b**). These
191 interventions did not alter acid resistance in *spoT*^{wt} cells, indicating that the defect is specific to
192 SpoT dysfunction. Notably, despite its ability to restore acid survival, ectopic expression of *gadE*
193 failed to improve the growth of *spoT*^{H414A} cells in M9Glc (**Extended Data Fig. 4c**). This

194 dissociation indicates that impaired acid resistance is not the primary cause of the growth defect,
195 which instead arises from glutamate starvation and broader metabolic misallocation.

196 We further examined acid tolerance across a range of pH values. In addition to catastrophic
197 sensitivity at pH 2.5, *spoT*^{H414A} cells exhibited reduced survival under mildly acidic conditions (pH
198 4.0–6.0) (**Fig. 4b, Extended Data Fig 4d**), consistent with the broader impairment of various acid
199 stress responses (**Extended Data Fig 4e**). Notably, these defects occurred despite preserved
200 viability under neutral conditions, indicating that SpoT-mediated basal regulation specifically
201 primes cells for acid stress rather than broadly supporting growth.

202 Intragenic suppressor mutations within *spoT* restore growth

203 The severe growth and acid resistance defects of *spoT*^{H414A} cells suggested that H414 of SpoT plays
204 a central regulatory role. To gain mechanistic insight into how SpoT activity is compromised by the
205 H414A substitution, we isolated spontaneous suppressor mutants capable of restoring growth of
206 *spoT*^{H414A} cells on M9Glc. After prolonged incubation (24–72 h), colonies of varying sizes emerged
207 on M9Glc agar (**Fig. 5a**).

208 Analysis of 50 independently isolated suppressors revealed that the strongest suppressors
209 predominantly carried secondary mutations within the *spoT* gene itself. Among large-colony
210 suppressors, we identified recurrent substitutions at residues G334 (G334S; supA), E364 (E364K;
211 supB), and S463 (S463R; sup41) as well as a small in-frame deletion within the synthetase domain
212 (sup17) (**Fig. 5b**). Whole-genome sequencing of smaller suppressors lacking *spoT* mutations
213 identified a single mutation in *rpoB* (K1262Q), which is likely similar as the previously described
214 stringent-response suppressors[39], and these were excluded from further analysis.

215 Reconstruction of the identified *spoT* suppressor mutations in a clean background fully restored
216 growth of *spoT*^{H414A} in M9Glc (**Extended Data Fig 5**), whereas deletion of *spoT* in the suppressor
217 strains abolished growth (**Fig. 5c**). These results demonstrate that intragenic mutations within SpoT
218 are both necessary and sufficient to suppress the *spoT*^{H414A} growth defect.

219 **Suppressor mutations restore acid resistance in proportion to growth recovery**

220 We next asked whether suppression of the growth defect was accompanied by restoration of acid
221 resistance. All four *spoT* suppressor strains exhibited improved survival under lethal acid challenge
222 (pH 2.5) compared to the parental *spoT*^{H414A} strain, although the degree of rescue varied (**Fig. 5d**).
223 The suppressor (sup41) displayed the most robust acid resistance, followed by supB, supA and
224 sup17.

225 Supplementation of the acid challenge medium with glutamate further enhanced survival across all
226 suppressor strains, with particularly pronounced effects in the weaker suppressors supB and sup17
227 (**Fig. 5d**). These differences suggest that the suppressor mutations restore SpoT function through
228 distinct mechanisms that differentially affect glutamate homeostasis and stress preparedness.

229 Thus, intragenic suppression of SpoT H414A simultaneously restores growth and acid resistance,
230 reinforcing the link between SpoT activity, metabolic balance, and stress survival.

231 **A sub-basal but non-zero level of ppGpp is sufficient for growth in minimal medium**

232 Given SpoT's role as a ppGpp synthase and hydrolase, we hypothesized that the growth defect of
233 *spoT*^{H414A} cells reflects insufficient ppGpp production and that suppressor mutations restore a
234 physiologically meaningful basal ppGpp pool. To test this, we measured intracellular ppGpp levels
235 using ^{32}P-orthophosphate labeling and thin-layer chromatography[40].

236 As expected, *spoT*^{H414A} cells produced barely detectable levels of ppGpp, whereas *spoT*^{wt} cells
237 accumulated a clear basal ppGpp signal (**Fig. 6a**). Surprisingly, suppressor strains did not exhibit a
238 marked increase in detectable ppGpp compared to *spoT*^{H414A} cells, suggesting that either very small
239 increases in ppGpp are sufficient for physiological rescue or that ppGpp turnover is highly dynamic
240 in these strains.

241 To directly test whether ppGpp synthesis is required for suppression, we inactivated the ppGpp
242 synthetase activity of SpoT (E319Q substitution) in the suppressor backgrounds. These mutations
243 dramatically delayed or abolished growth recovery in M9Glc (**Fig. 6b**), demonstrating that ppGpp
244 synthesis is essential for suppression. Conversely, inactivation of SpoT's hydrolase activity (H72A
245 D73A substitution) led to clear accumulation of ppGpp (**Fig. 6c**) and accelerated growth resumption
246 (**Fig. 6d**), indicating that suppressor strains produce ppGpp that is rapidly degraded. Notably, the
247 hydrolase-inactive (SYN) variants of supA and sup17 could not be obtained, likely due to the
248 toxicity of high ppGpp level.

249 Together, these data demonstrate that a sub-basal but non-zero ppGpp pool, below the detection
250 limit of conventional assays, is sufficient to support growth in minimal medium and that SpoT
251 activity is finely tuned to maintain this pool.

252 Consistent with this model, systematic truncation of SpoT C-terminal regulatory domains revealed
253 that distinct suppressor mutations alter the contribution of individual domains to growth control
254 (**Extended Data Fig. 6**), without abolishing the requirement for basal ppGpp synthesis. These
255 findings indicate that SpoT H414 functions within a broader intramolecular regulatory network that
256 fine-tunes basal ppGpp production rather than acting as an isolated molecular switch.

257 **Basal ppGpp negatively regulates SpoT abundance**

258 To investigate how SpoT activity is regulated, we examined SpoT protein levels using an antiserum
259 raised against the C-terminal regulatory domains of SpoT. Immunoblot analysis revealed that SpoT
260 protein levels were substantially elevated in *spoT*^{H414A} cells compared to *spoT*^{wt} and suppressor
261 strains (**Fig. 6e**).

262 Because *spoT*^{H414A} cells produce sub-basal ppGpp levels, whereas suppressor strains restore
263 physiological function with marginally increased ppGpp, these results suggest that basal ppGpp
264 negatively regulates SpoT abundance through a feedback mechanism. Such feedback would
265 stabilize intracellular ppGpp levels by adjusting SpoT protein concentration in response to alarmone
266 availability. This regulatory logic provides a mechanistic explanation for how SpoT maintains a
267 narrow basal ppGpp range sufficient for metabolic homeostasis without triggering a full stringent
268 response.

269 **Suppressor mutations differentially restore global transcriptional programs**

270 To understand how suppressor mutations restore growth and acid resistance, we performed RNA
271 sequencing on the four suppressor strains. Both parallel coordinates and multidimensional scaling
272 analysis revealed that strong suppressors (supA and sup41) clustered closely with *spoT*^{wt} cells,
273 whereas weaker suppressors (supB and sup17) occupied intermediate positions between *spoT*^{H414A}
274 and *spoT*^{wt} (**Extended Data Fig. 7a,7b**).

275 Consistent with their physiological phenotypes, strong suppressors (supA and sup41) largely
276 restored expression of acid resistance genes and repressed phage shock and SOS response pathways
277 (**Extended Data Fig. 7c,7d**). In contrast, weaker suppressors (supB and sup17) exhibited partial
278 correction of these transcriptional defects (**Extended Data Fig. 8**). Across all suppressors, a core
279 set of genes involved in amino acid metabolism and stress adaptation was consistently restored

280 (**Extended Data Fig. 7c**), whereas genes aberrantly induced in *spoT*^{H414A} cells were broadly
281 repressed (**Extended Data Fig. 7d**).

282 These results indicate that suppressor mutations restore SpoT-dependent basal regulation in a
283 graded manner, with transcriptional recovery correlating with physiological rescue.

284 **SpoT H414 function is conserved in enteric pathogens**

285 Finally, we asked whether the regulatory role of SpoT H414 is conserved in pathogenic
286 enterobacteria. We introduced the corresponding H414A substitution into SpoT homologs from
287 *Salmonella enterica* serovar Typhimurium and *Shigella flexneri* and expressed these proteins in an
288 *E. coli* ppGpp^0 background.

289 Wild-type SpoT homologs from both species fully restored growth in M9Glc and acid resistance
290 when expressed in an *E. coli* ppGpp^0 background, whereas the corresponding H414A variants failed
291 to support either phenotype (**Fig. 7a–d**). Notably, glutamate supplementation rescued both growth
292 and acid resistance defects in the *Shigella* SpoT H414A strain but not in the *Salmonella* SpoT
293 H414A variant. This differential rescue correlates with the degree of sequence divergence in
294 regulatory regions of SpoT. *S. flexneri* SpoT differs from *E. coli* SpoT at only a single conserved
295 position (A614G) within the CC domain, whereas *S. Typhimurium* SpoT shares 98.15% overall
296 identity but contains multiple amino acid substitutions distributed across the C-terminal domains,
297 including a cluster of nine substitutions within linker-2 between TGS and CC domains (**Extended**
298 **Data Fig. 9**). These differences likely modulate intramolecular regulatory interactions within SpoT,
299 thereby influencing the ability of the H414A variants to respond to glutamate supplementation.

300 Altogether, these results demonstrate that SpoT H414 plays a conserved role in coordinating growth
301 and acid resistance across enteric pathogens, underscoring its physiological and evolutionary
302 significance.

303 **Discussion**

304 **Basal ppGpp defines a distinct regulatory regime coordinating metabolism and stress**
305 **resistance**

306 The stringent response has classically been viewed as an acute adaptation to amino acid starvation,
307 driven by RelA-dependent bursts of ppGpp that globally reprogram transcription and metabolism
308 (**Fig. 7e**, top). Our findings reveal a complementary and previously underappreciated role for SpoT-
309 derived basal ppGpp as a distinct regulatory regime that operates independently of acute starvation
310 signalling (**Fig. 7e**, middle). By dissecting the function of a conserved SpoT residue (H414), we
311 show that maintenance of a sub-basal yet non-zero ppGpp pool is essential for metabolic
312 homeostasis, growth in minimal medium, and survival under extreme acid stress.

313 Importantly, the defects observed in *spoT*^{H414A} cells are not attributable to an inability to mount a
314 canonical stringent response. Rather, they reflect a failure to maintain basal regulatory control over
315 metabolic flux allocation and stress preparedness (**Fig. 7e**, bottom). This distinction expands the
316 conceptual framework of ppGpp signalling, positioning SpoT not merely as a backup or modulator
317 of RelA activity, but as a primary regulator of foundational physiological states.

318 **SpoT-mediated control of glutamate homeostasis integrates growth and acid resistance**

319 A central finding of this study is that SpoT H414 is required to prevent misallocation of metabolic
320 resources that leads to glutamate depletion. Transcriptomic analysis revealed strong and

321 coordinated induction of the arginine biosynthesis pathway, which directly consumes glutamate,
322 alongside upregulation of *de novo* purine nucleotide biosynthesis, which indirectly drains glutamate
323 through increased glutamine demand. Genetic and physiological experiments establish arginine
324 biosynthesis as the dominant driver of glutamate depletion, while purine biosynthesis likely
325 exacerbates this imbalance.

326 Glutamate occupies a unique position in bacterial physiology, serving as a key metabolic hub and as
327 the essential substrate for the glutamate-dependent Gad acid resistance system. Consequently,
328 glutamate depletion provides a unifying explanation for both the growth defect and catastrophic
329 acid sensitivity observed in $spoT^{H414A}$ cells. The ability of glutamate supplementation or genetic
330 blockade of arginine biosynthesis to restore growth, together with GadE-dependent rescue of acid
331 resistance, underscores the centrality of glutamate homeostasis in SpoT-mediated regulation.

332 **Basal ppGpp tunes stress preparedness rather than viability**

333 Our data demonstrate that SpoT-derived basal ppGpp does not simply support cell viability, but
334 instead primes cells for environmental stress. Despite severe repression of acid resistance genes,
335 $spoT^{H414A}$ cells remain viable under neutral, well-buffered conditions, indicating that SpoT H414 is
336 specifically required for stress preparedness rather than basal survival. This distinction explains
337 why growth defects and acid resistance defects, while mechanistically linked through glutamate
338 homeostasis, manifest under different environmental conditions.

339 Notably, RelA is dispensable for acid resistance under the conditions tested, highlighting a division
340 of labor between stringent response enzymes: RelA mediates acute starvation responses, whereas
341 SpoT maintains basal regulatory states necessary for survival in fluctuating environments.

342 **SpoT intrinsically tunes a narrow basal ppGpp window**

343 Intragenic suppressor analysis reveals that SpoT encodes an intrinsic regulatory module capable of
344 fine-tuning basal ppGpp levels. Suppressor mutations distributed across both the catalytic and
345 regulatory regions of SpoT restore growth and acid resistance without producing large, readily
346 detectable increases in ppGpp, indicating that very low, rapidly turned-over ppGpp pools are
347 physiologically sufficient for function.

348 Perturbation of SpoT's enzymatic balance further supports this model. Inactivation of ppGpp
349 synthesis abolishes suppression, whereas inactivation of hydrolase activity elevates ppGpp levels
350 and accelerates growth recovery. Together, these results demonstrate that SpoT actively maintains a
351 narrow basal ppGpp range and that deviations below this threshold have profound physiological
352 consequences.

353 Consistent with this quantitative tuning model, systematic truncation of SpoT C-terminal regulatory
354 domains revealed that distinct suppressor mutations differentially alter the contribution of
355 individual domains to growth control, without abolishing the requirement for basal ppGpp
356 synthesis. These findings indicate that SpoT H414 functions within a broader intramolecular
357 regulatory network that modulates ppGpp production in a graded manner rather than acting as a
358 binary on–off switch.

359 Finally, the observed negative correlation between basal ppGpp levels and SpoT protein abundance
360 suggests the existence of a feedback mechanism that stabilizes this regulatory regime. Such
361 feedback would allow cells to dynamically adjust SpoT abundance and activity to maintain
362 metabolic balance without triggering a full stringent response.

363 **Conservation of SpoT H414 underscores physiological relevance**

364 The functional conservation of SpoT H414 in *Salmonella* and *Shigella* underscores the broader
365 significance of basal ppGpp regulation in enteric bacteria. While species-specific differences in
366 SpoT regulatory domains modulate the extent to which glutamate supplementation can compensate
367 for H414A dysfunction, the core requirement for this residue in supporting growth and acid
368 resistance is conserved. This conservation highlights basal ppGpp as a fundamental determinant of
369 bacterial fitness in acidic environments, such as those encountered during host colonization.

370 **Implications and outlook**

371 Together, our findings establish SpoT as a central coordinator of metabolic homeostasis and stress
372 resistance through maintenance of a basal ppGpp pool. This regulatory regime operates
373 independently of the acute, RelA-mediated stringent response and integrates amino acid metabolism
374 with acid resistance, thereby enabling bacterial survival under hostile environmental conditions.

375 Several important questions remain. Our domain truncation and suppressor analyses indicate that
376 SpoT H414 functions within a distributed intramolecular regulatory network that quantitatively
377 tunes basal ppGpp production, rather than acting as a simple on–off switch; however, the precise
378 nature of the signal sensed by H414, whether metabolic, physicochemical, or intramolecular,
379 remains unresolved. In addition, defining the absolute intracellular ppGpp concentrations required
380 for basal regulation will require new methodologies capable of resolving low-abundance alarmone
381 pools with high temporal resolution, ideally through single-cell reporters coupled to dynamic
382 growth measurements. More broadly, elucidating how basal ppGpp differentially modulates
383 specific metabolic and stress-response pathways will be essential for fully understanding this
384 regulatory logic.

385 Given the central role of acid resistance in enteric pathogenesis, SpoT-mediated basal ppGpp
386 regulation represents a potential vulnerability that could be exploited to compromise bacterial
387 survival. More generally, our work highlights the physiological importance of low-level signaling
388 states and suggests that basal regulatory regimes may play underappreciated roles in coordinating
389 metabolism and stress adaptation across diverse microbial systems.

390 **Figures and legends**

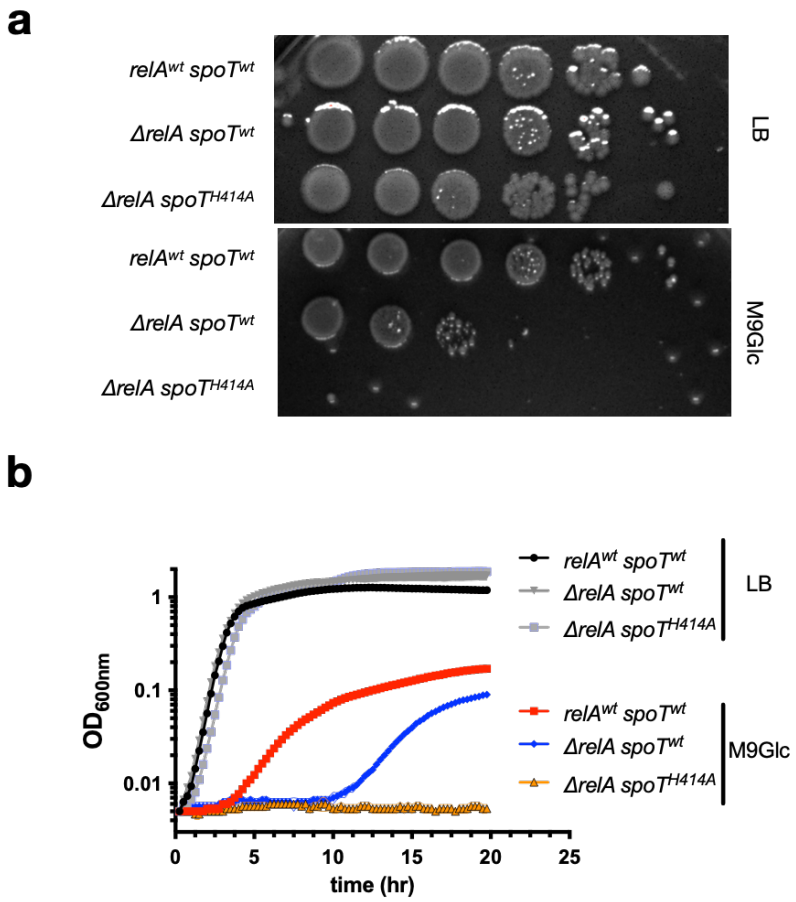

391

392 **Figure 1. A conserved SpoT H414A mutation reveals defective growth on M9Glc medium. (a)**

393 Growth of wild type *E. coli* MG1655 (*relA*^{wt} *spoT*^{wt}), and Δ*relA spoT*^{H414A}, Δ*relA spoT*^{wt} strains on

394 LB and M9Glc solid media. **(b)** Growth dynamics of the same strains in liquid LB and M9Glc media.

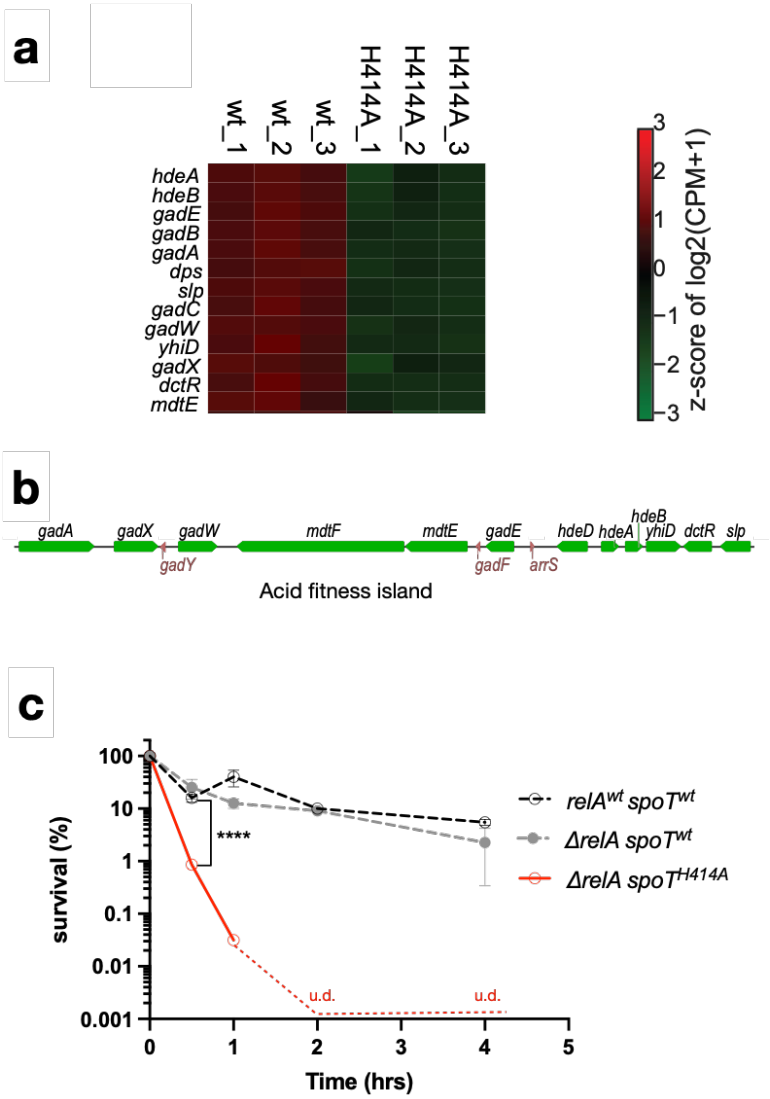

Figure 2. Transcriptomic analysis reveals collapse of acid resistance programs. (a) Heatmap of genes encoded in the *E. coli* acid fitness island in *spoT*^{H414A} relative to *spoT*^{wt}. **(b)** Genetic organization of the *E. coli* acid fitness island. (**c**) Acid resistance assay of wild type MG1655 (*relA*^{wt} *spoT*^{wt}), Δ*relA spoT*^{H414A} and Δ*relA spoT*^{wt}. Survival of indicated strains following challenge at pH 2.5, expressed as the percentage of colony-forming units (CFUs) remaining relative to starting CFUs for each strain. Data are means ± s.d. from biological replicates. u.d., undetectable. Statistical significance was assessed using unpaired two-tailed Student's *t*-tests. **** denote $P < 0.0001$.

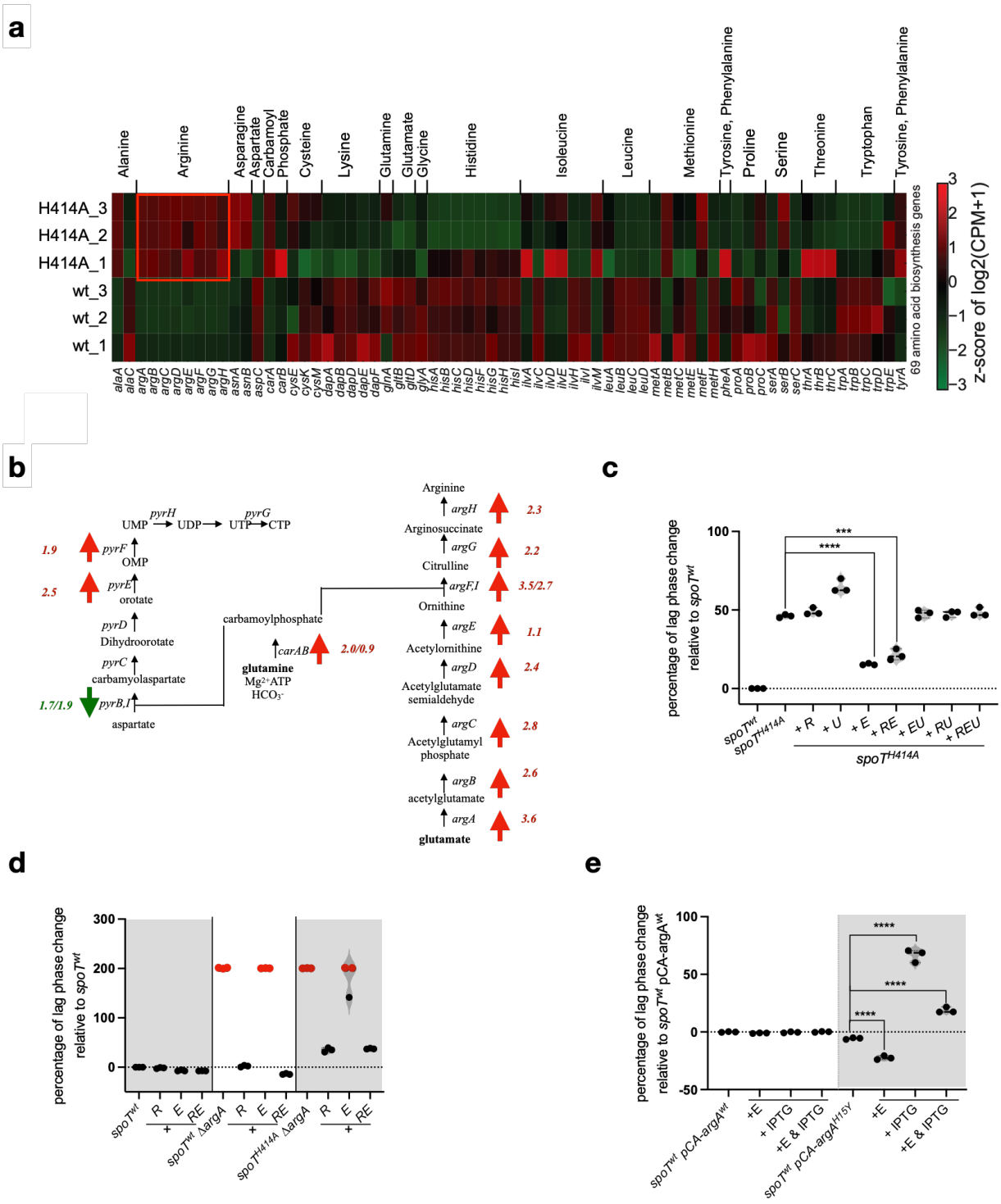

404

405 **Figure 3. Arginine metabolic overflow drives glutamate depletion in *spoT*^{H414A}. (a)** Heatmap of

406 genes involved in amino acid biosynthesis, comparing *spoT*^{H414A} and *spoT*^{wt} strains. The arginine

407 biosynthesis genes are highlighted. **(b)** Schematic of the arginine biosynthesis pathway in *E. coli*.

408 Genes upregulated in *spoT*^{H414A} cells are indicated by red upward arrows, accompanied by average
409 $\log_2$ fold-change values relative to *spoT*^{wt}. **(c)** Normalized lag phase duration of *spoT*^{H414A} cells
410 grown in M9Glc medium with supplementation of arginine (5.2 mM, R), uracil (0.2 mM, U),
411 glutamate (0.6 mM, E), or the indicated combinations, expressed relative to the *spoT*^{wt} strain. **(d)**
412 Normalized lag phase duration of indicated strains grown in M9Glc medium with supplementation
413 of arginine (R), glutamate (E), or both, relative to *spoT*^{wt}. Red dots indicate failure to resume
414 growth within the 72-h observation window. **(e)** Normalized lag phase duration of *spoT*^{wt} strains
415 harboring pCA24N-*argA*^{wt} or the feedback-resistant pCA24N- *argA*^{H15Y} allele, grown with or
416 without IPTG induction and/or glutamate supplementation (0.6 mM), relative to the uninduced
417 *argA*^{wt} control. Data are means ± s.d. from biological replicates. Statistical significance was
418 assessed using unpaired two-tailed Student's *t*-tests. ****, *** denote $P < 0.0001$ and 0.001,
419 respectively.

420

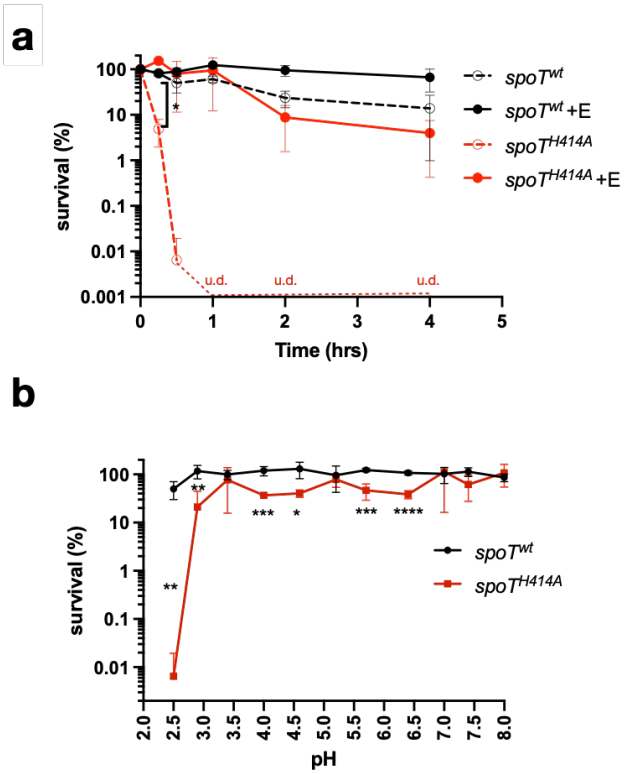

Figure 4. SpoT H414 is required for survival under extreme acid stress.

(a) Acid resistance assay of Δ*relA spoT*^{H414A} and Δ*relA spoT*^{wt} as in Figure 2c. Where indicated (+E), glutamate (0.6 mM) was included in the acid challenge medium. u.d., undetectable. **(b)** Survival of *spoT*^{H414A} and *spoT*^{wt} strains following 30 min challenge in buffers adjusted to the indicated pH values, normalized to starting CFUs. Data are means ± s.d. from biological replicates. Statistical significance was assessed using unpaired two-tailed Student's *t*-tests. ****, ***, **, * denote $P < 0.0001$, 0.001, 0.01, and 0.05, respectively.

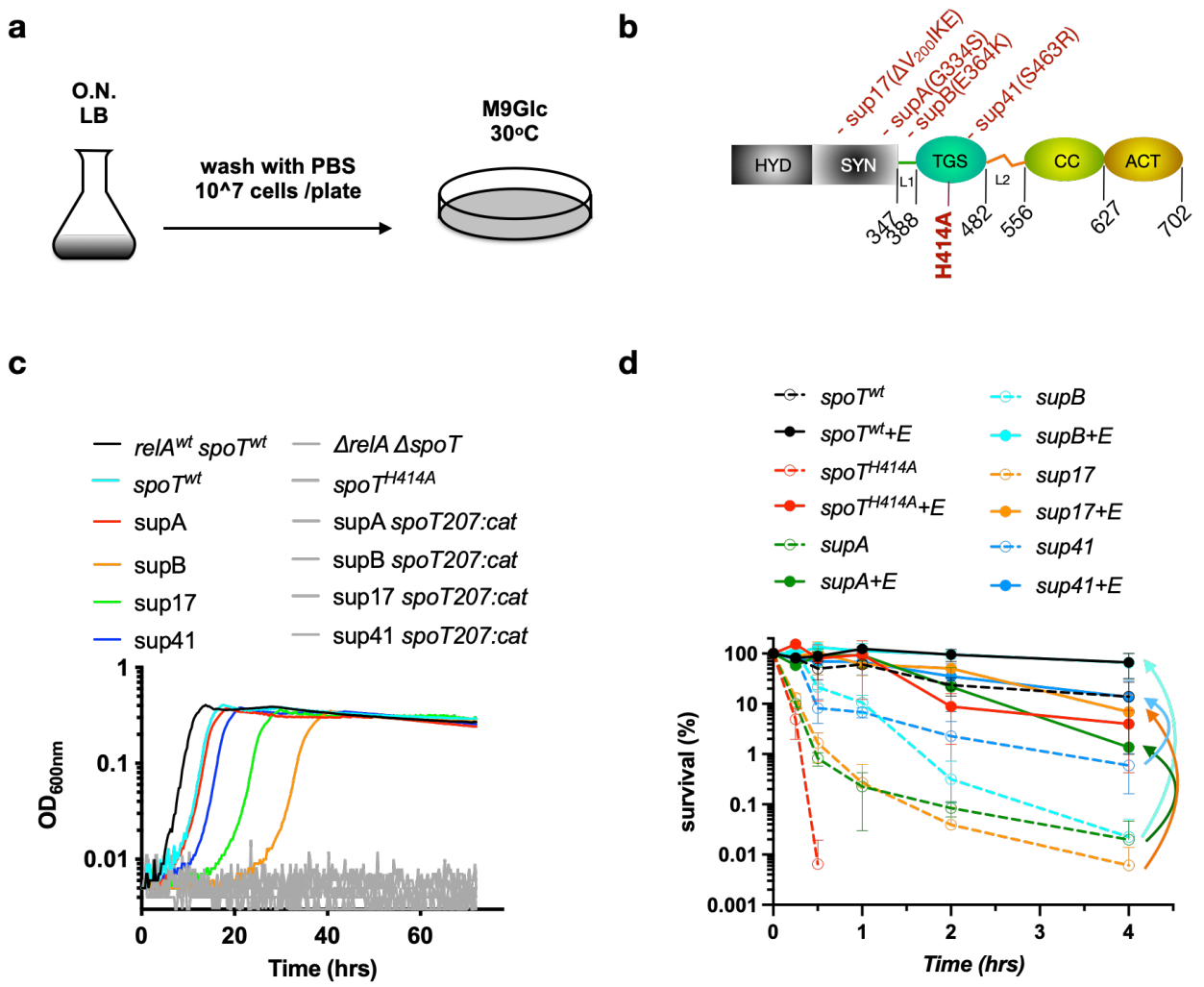

Figure 5. Intragenic SpoT suppressor mutations restore growth and acid resistance. (a) Schematic illustrating the isolation of spontaneous suppressor mutations that enable growth of *spoT*^{H414A} cells on M9Glc medium. **(b)** Domain architecture of the SpoT protein, indicating the locations of suppressor mutations. Amino-acid positions are shown below. L1/L2, linker-1/linker-2; HYD, hydrolase domain; SYN, synthetase domain; TGS, ThrRS–GTPase–SpoT domain; CC, conserved cysteine domain; ACT, aspartate kinase–chorismate mutase–TyrA domain. **(c)** Growth dynamics of four suppressor strains (supA, supB, sup17, sup41) compared with *spoT*^{H414A}, *spoT*^{wt}, ppGpp^{0} (*ΔrelA ΔspoT*), and wild-type MG1655 (*relA*^{wt} *spoT*^{wt}). Also shown are suppressor strains in which *spoT* was deleted (*spoT207::cat*). **(d)** Survival of indicated strains following challenge at

440 pH 2.5, expressed as normalized CFUs. Where indicated (+E), glutamate (0.6 mM) was included.

441 Data are means ± s.d. Statistical significance was assessed using unpaired two-tailed Student's *t*-

442 tests. ***, **, * denote $P < 0.001$, 0.01, and 0.05, respectively.

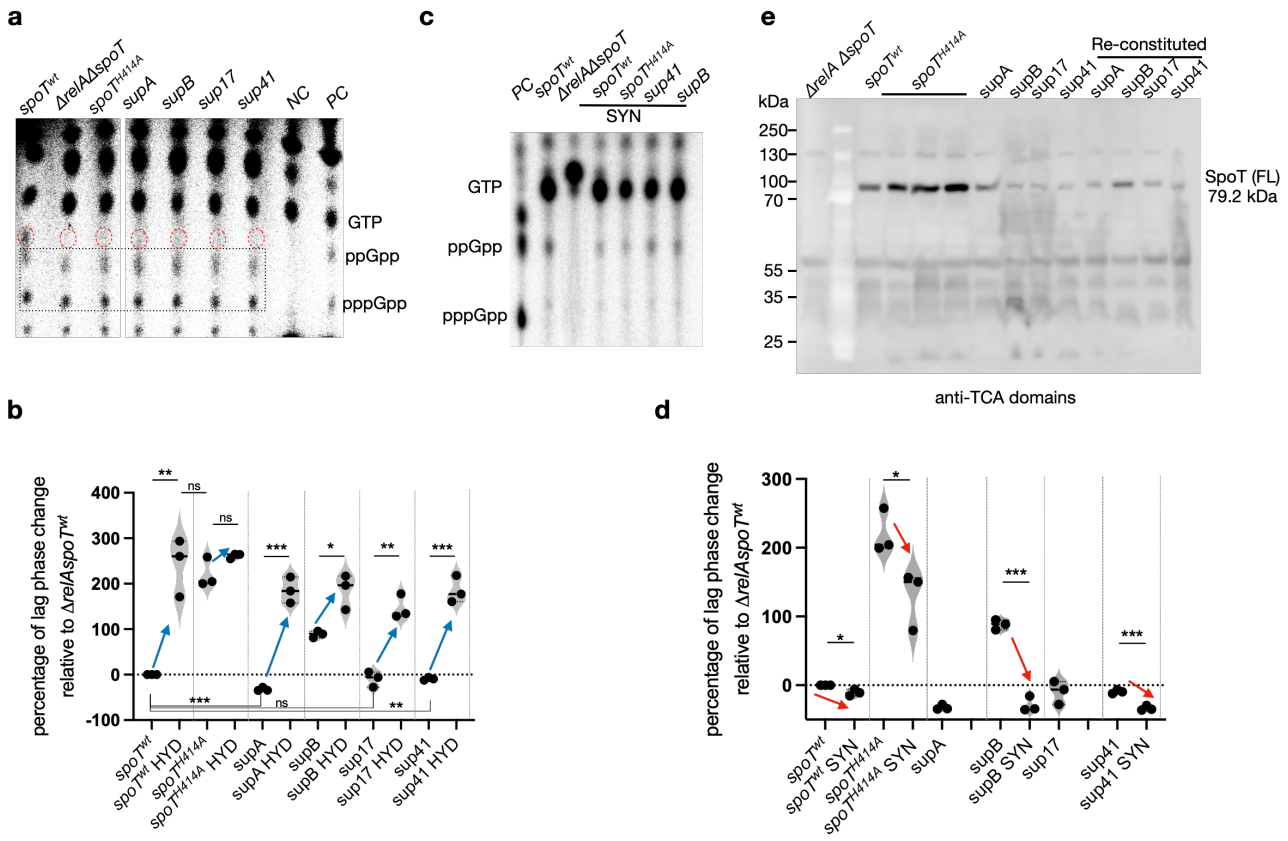

443

444 **Figure 6. A sub-basal ppGpp pool is sufficient for physiological function. (a)** Thin-layer

445 chromatography (TLC) analysis of ^{32}p-labeled nucleotides from indicated strains grown in low-

446 phosphate MOPS minimal medium supplemented with 0.2% glucose. NC and PC denote *ΔrelA*

447 *ΔspoT* and valine-treated wild-type MG1655 controls, respectively. Red circles mark ppGpp; boxed

448 regions indicate nonspecific spots also present in *ΔrelA ΔspoT* samples. **(b)** Effect of inactivating

449 SpoT ppGpp synthetase activity (E319Q; HYD) on growth recovery in M9Glc. Lag phase duration

450 is normalized to *spoT*^{wt}. **(c)** TLC analysis of ^{32}p-labeled nucleotides from strains carrying SpoT

451 hydrolase-inactive mutations (H72A D73A; SYN). **(d)** Growth recovery of hydrolase-inactive

452 strains (SYN), quantified as normalized lag phase duration relative to *spoT*^{wt}. Note that the
453 hydrolase-inactive (SYN) variants of supA and sup17 could not be obtained, thereby not tested. **(e)**
454 Immunoblot analysis of SpoT protein levels using an antiserum raised against the SpoT C-terminal
455 (TGS–CC–ACT; anti-TCA) region. Cells were grown in M9Glc to early exponential phase
456 ($OD_{600nm} \approx 0.2$) prior to sampling. *spoT*^{H414A} samples were collected after prolonged incubation, as
457 in Extended Data Fig. 1c. *ΔrelA ΔspoT* cells grown in LB served as a negative control.

458

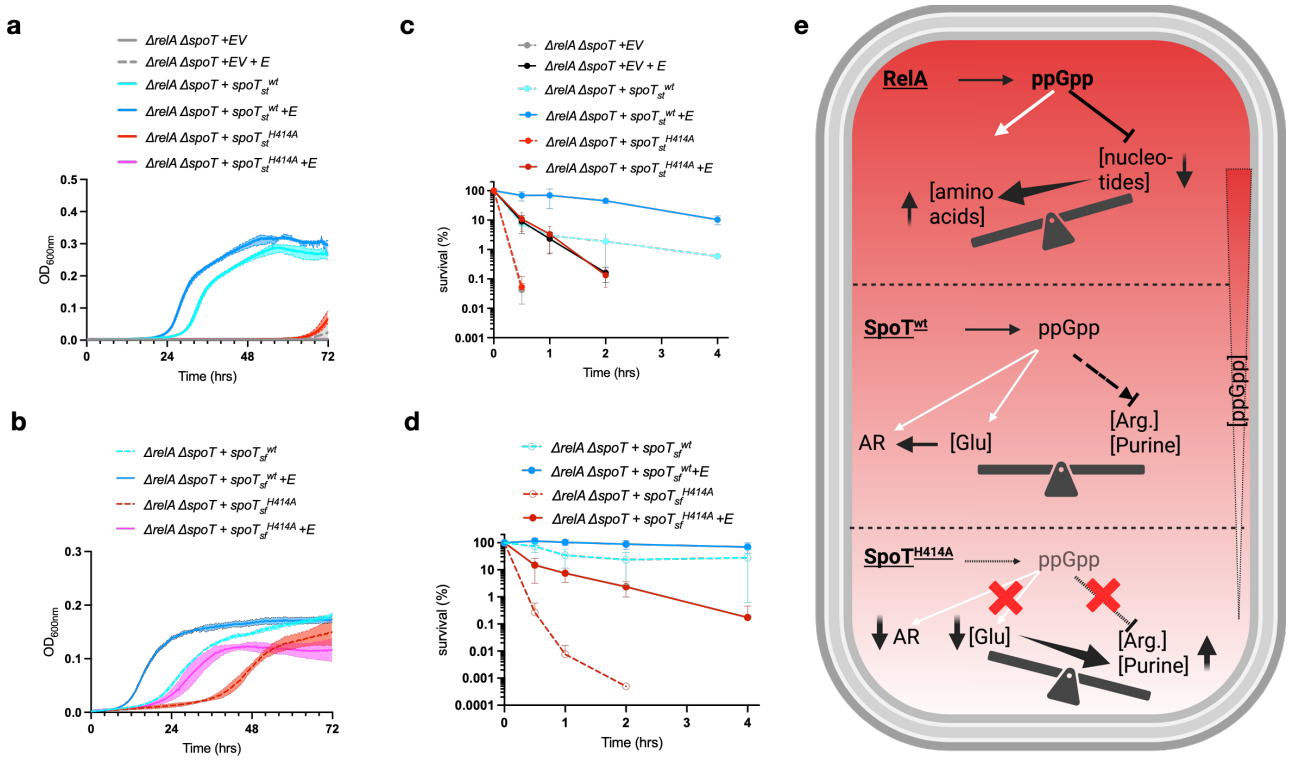

459

460 **Figure 7. Conservation of SpoT H414 function and model for basal ppGpp regulation. (a,b)**
461 Growth of *E. coli* ppGpp^0 strains complemented with SpoT homologs from *Salmonella enterica*
462 serovar Typhimurium (**a**) or *Shigella flexneri* (**b**). E, glutamate (0.6 mM); EV, empty vector. Data
463 represent at least three biological replicates. **(c,d)** Survival of complemented ppGpp^0 strains
464 (*Salmonella* (**c**) or *Shigella* (**d**)) following challenge at pH 2.5, normalized to starting CFUs. Where

465 indicated (+E), glutamate (0.6 mM) was included. **(e)** Under acute amino-acid starvation (top),
466 RelA is rapidly activated by ribosome-associated signals to generate a high-amplitude ppGpp surge,
467 globally reprogramming transcription and metabolism to suppress nucleotide pathways and promote
468 amino-acid availability. Under minimal medium growth (middle), SpoT maintains a low but
469 physiologically essential basal ppGpp pool that is distinct from and independent of RelA. This basal
470 ppGpp state coordinates metabolic homeostasis by restraining excessive arginine and purine
471 biosynthesis, preserving intracellular glutamate levels, and priming multiple acid resistance
472 programs, including the glutamate-dependent Gad system (AR). In *spoT*^{H414A} cells (bottom), a sub-
473 basal level of ppGpp remains below the threshold required for effective metabolic and stress
474 control. Therefore, arginine and purine biosynthetic pathways become overactivated, intracellular
475 glutamate is depleted, and acid resistance programs are inadequately induced, resulting in growth
476 failure in minimal medium and extreme sensitivity to acid stress.

477

EXTENDED DATA FIGURE LEGENDS

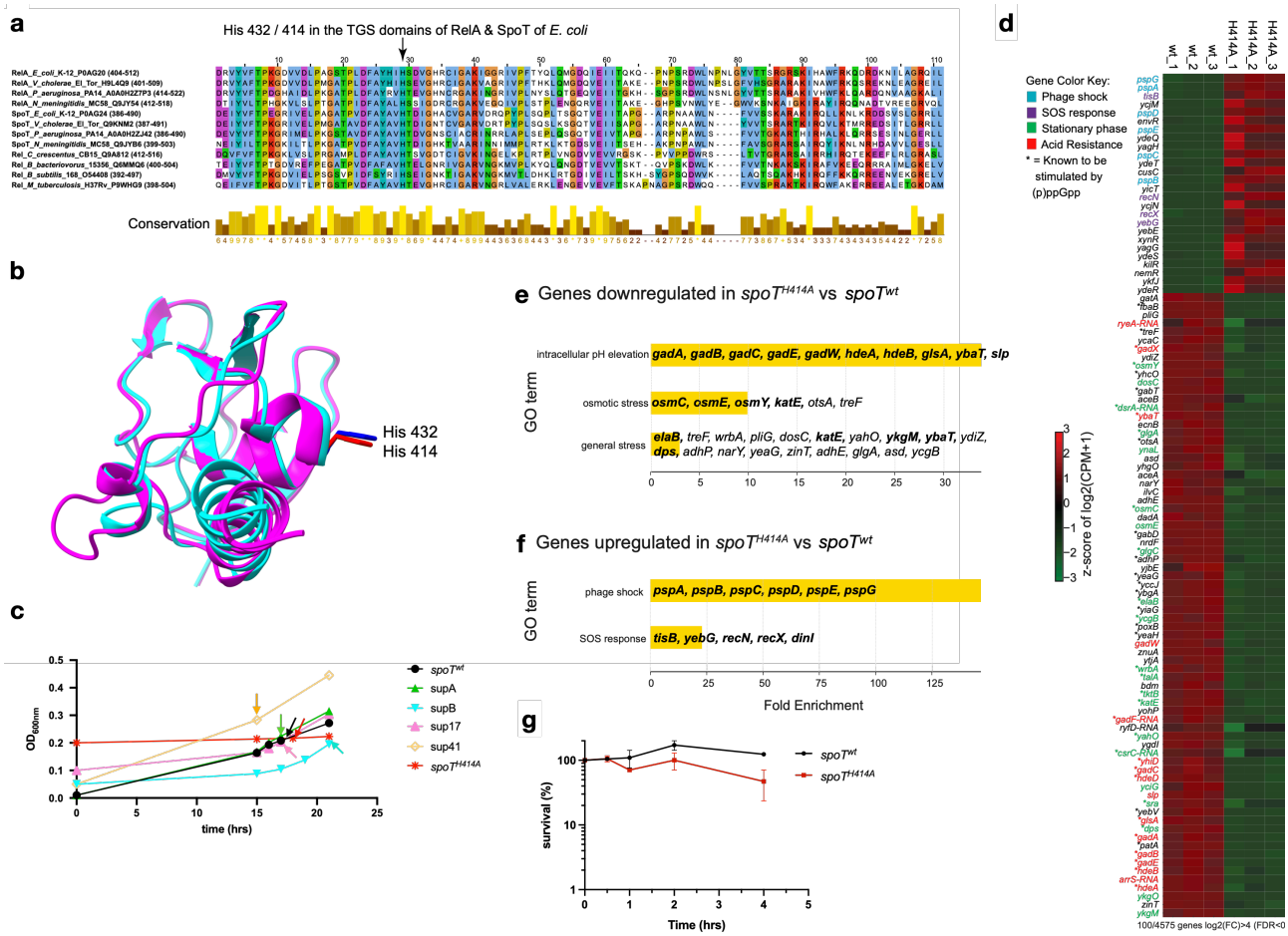

Extended Data Fig. 1 (a) Sequence alignment of 12 TGS domains of RelA, SpoT and their homologous proteins from α, β, γ and δ proteobacteria, Firmicute and Actinomycete. The highly conserved position corresponding to His 432 of RelA and 414 of SpoT of *E. coli* is indicated with an arrow. **(b)** Superpositioning of the TGS domains of RelA and SpoT from *E. coli* (rmsd over 91 of 98 atom pairs is 0.762 Å) generated by AF3. **(c)** Representative growth curves of Δ*relA spoT*^{H414A}, Δ*relA spoT*^{wt} and the four suppressor strains in M9Glc media for collecting RNA sequencing samples. Cells were collected when their OD_{600nm} approach ca. 0.2, except for *spoT*^{H414A} cells, which could not grow in this medium, thus these cells were collected after incubated for 18 hrs in the same medium. Coloured arrows indicate the sampling points for each strain. **(d)** Heatmap

of genes with greater than 16-fold changes between Δ*relA spoT*^{H414A} and Δ*relA spoT*^{wt} cells growing in M9Glc medium. **(e)** Gene ontology groups of genes downregulated in the *spoT*^{H414A} strain. Genes downregulated at least 16-fold were extracted using DEGUST (|Log2(FC)| > 4; FDR < 0.05) and analysed by AmiGO and Panther. The 58 genes downregulated more than 16-fold (Log2(FC) < -4) are listed in **Table S3**. **(f)** Gene ontology groups of genes upregulated at least 16-fold in the *spoT*^{H414A} strain. The 28 genes upregulated more than 16-fold (Log2(FC) > 4) are listed in **Table S3**. Note the differences in the Fold Enrichment scales in **(e)** and **(f)**. Gene names in bold in (**e, f**) are strongly up or downregulated. **(g)** Normalized percentage of surviving viable cells of the *spoT*^{wt} and *spoT*^{H414A} strains growing in M9Glc medium. Two replicates were performed and presented.

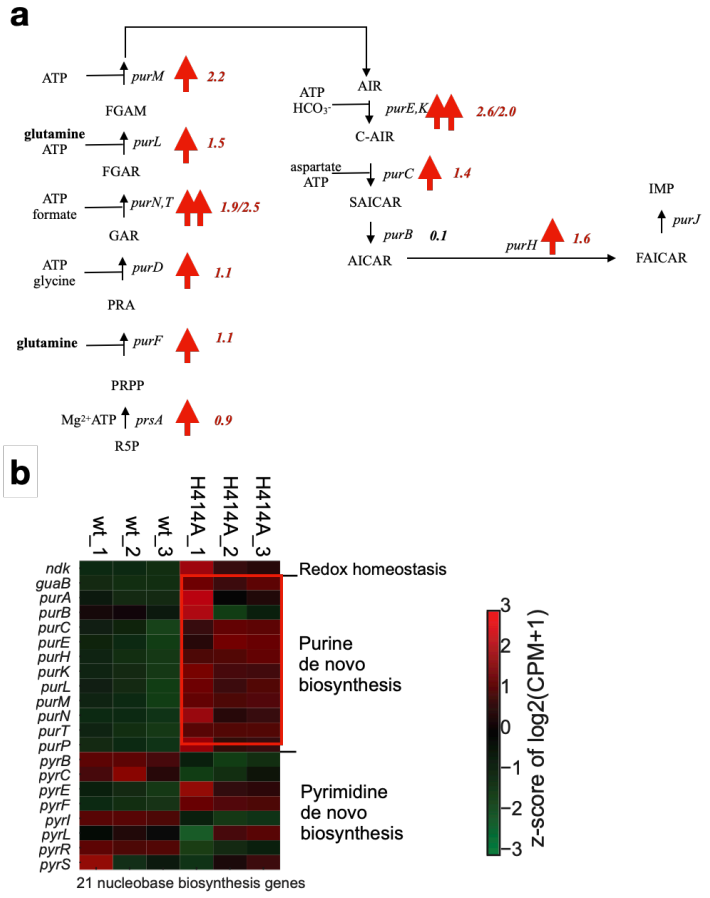

499 **Extended Data Fig. 2 (a)** Purine nucleotide de novo biosynthesis pathway in *E. coli*. The
500 upregulated genes are indicated by a red upward arrow alongside average log2(FC) values of
501 *spoT*^{H414A} versus *spoT*^{wt}. R5P, ribose-5-phosphate; PRPP, 5-phosphoribosyl 1-pyrophosphate; PRA,
502 5-phosphoribosylamine; GAR, 5'-phosphoribosylglycinamide; FGAR, 5'-phosphoribosyl-N-
503 formylglycineamide; FGAM, 5'-phosphoribosylformylglycinamidine; AIR, 5-aminoimidazole
504 ribonucleotide; C-AIR, 5-carboxyamino-1-(5-phospho-D-ribosyl)imidazole; SAICAR, 1-(5-
505 phosphoribosyl)-4-(N-succino-carboxamide)-5-aminoimidazole; AICAR, 5-amino-1-(5-phospho-D-
506 ribosyl)imidazole-4-carboxamide; FAICAR, 5-formamido-1-(5-phospho-D-ribosyl)imidazole-4-
507 carboxamide; IMP, inosine 5'- monophosphate. **(b)** Heatmap of genes involved in purine and
508 pyrimidine nucleotide de novo biosynthesis. The red box indicates purine de novo biosynthesis
509 genes.

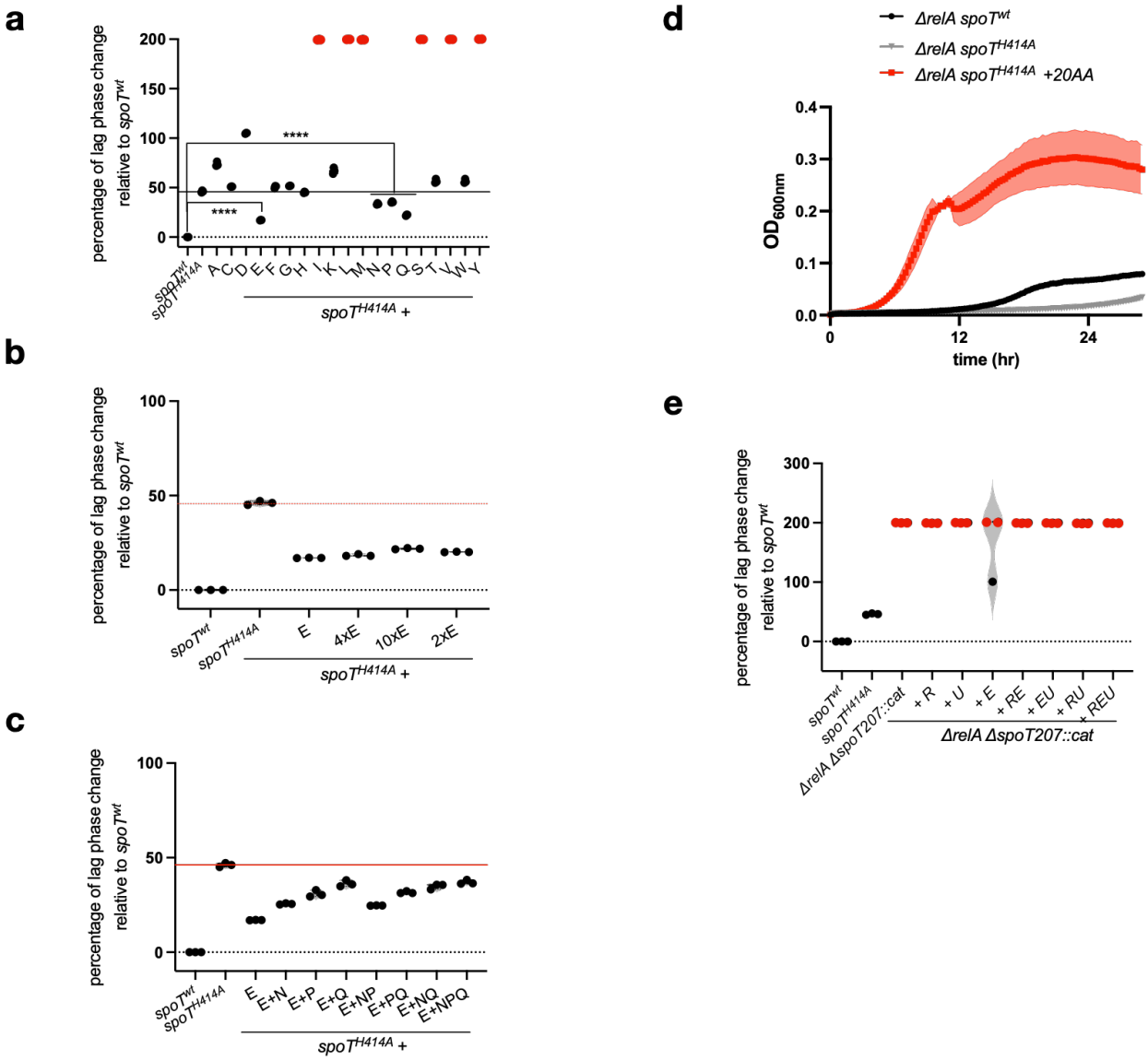

Extended Data Fig. 3 (a) Normalized lag phase length of the *spoT*^{H414A} strain without or with supplemented each of the 20 amino acids (in single letters; A, alanine 0.8mM; C, cysteine 0.1mM; D, aspartic acid 0.4mM; E, glutamate 0.6mM; F, phenylalinine 0.4mM; G, glycine 0.8mM; H, histidine 0.2mM; I, isoleucine 0.4mM; K, lysine 0.4mM; L, leucine 0.8mM; M, methionine 0.2mM; N, asparigine 0.4mM; P, proline 0.4mM; Q, glutamine 0.6mM; R, arginine 5.2mM; S, serine 10mM; T, threonine 0.4mM; V, valine 0.6mM; W, tryptophan 0.1mM; Y, tyrosine 0.2mM), relative to the *spoT*^{wt} strain in M9Glc medium. **(b)** Normalized lag phase length of the *spoT*^{H414A} strain without or with supplemented 1x, 2x, 4x, 10x glutamate (E, 1x = 0.6 mM), relative to the *spoT*^{wt} strain in M9Glc

medium. **(c)** Normalized lag phase length of the *spoT*^{H414A} strain without or with supplemented glutamate (0.6 mM) together with glutamine (Q, 0.6 mM), proline (P, 0.4 mM), asparagine (N, 0.4 mM), relative to the *spoT*^{wt} strain in M9Glc medium. **(d)** Representative growth curves of Δ*relA spoT*^{H414A}, Δ*relA spoT*^{wt} strains without or with all 20 amino acids (+20AA) (see method for details) in M9Glc medium. Two biological replicates each with two technical replicates were performed and presented. **(e)** Normalized lag phase length of the Δ*relA*Δ*spoT207::cat* (ppGpp^0) strain without or with supplemented arginine (5.2 mM, R), uracil (0.2 mM, U), glutamate (0.6 mM, E) or their varied combinations, relative to the *spoT*^{wt} strain in M9Glc medium. Red dots indicate fails of regrowth within the tested time range of 72 hrs.

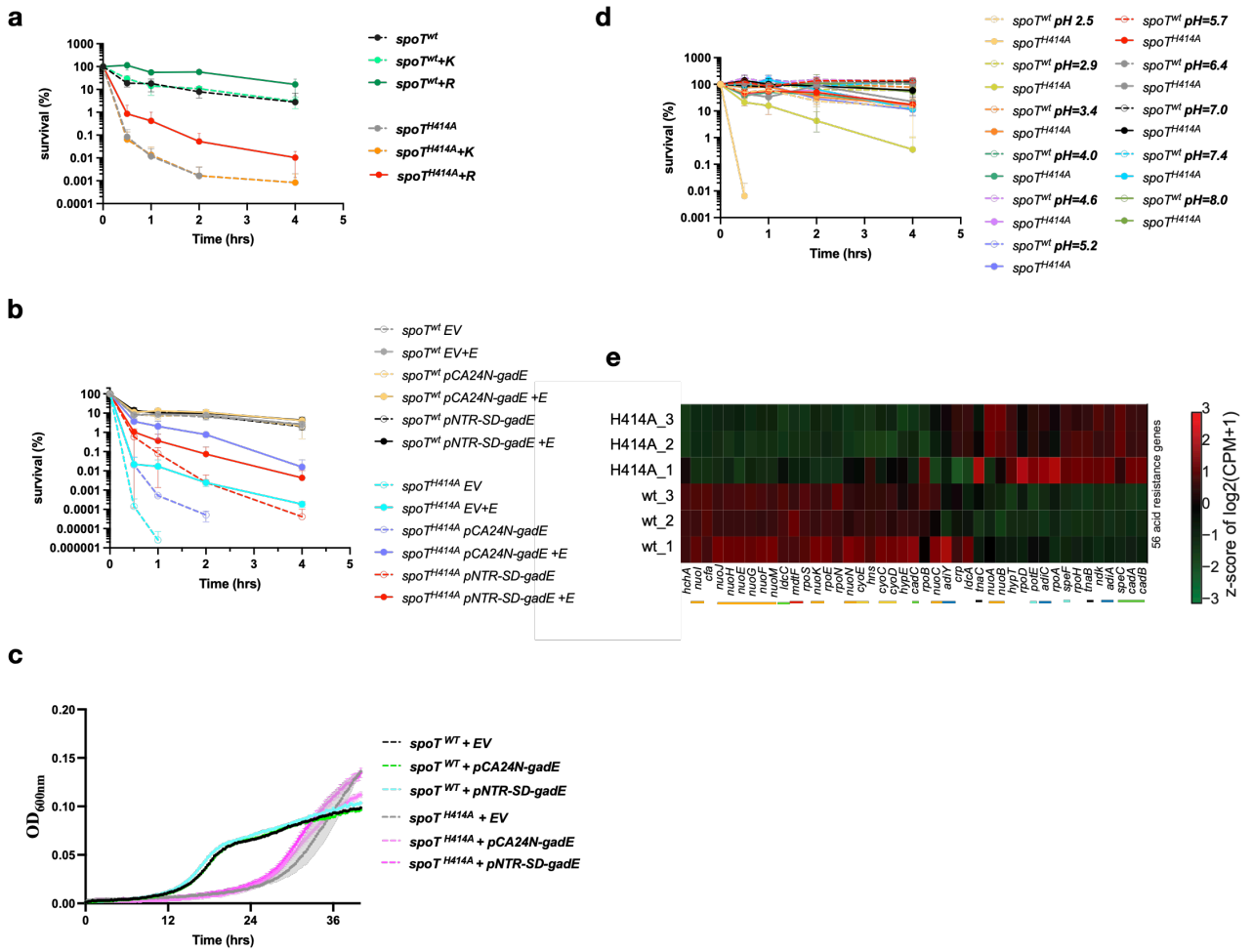

529 **Extended Data Fig. 4 (a)** Normalized percentage of surviving cells of various strains after
530 challenged with pH=2.5. The data were normalized to the starting CFUs of each respective tested
531 strain. +K, +R, lysine (0.6 mM), arginine (0.6 mM) included in the pH=2.5 medium, respectively.
532 **(b)** Normalized percentage of surviving cells of *spoT*^{wt} or *spoT*^{H414A} strains containing various
533 plasmid vectors (pCA24N [41], pNTR-SD [42]) after challenged with pH=2.5. The data were
534 normalized to the starting CFUs of each respective tested strain. EV, empty vector pCA24N. +E,
535 glutamate (0.6 mM) included in the pH=2.5 medium. **(c)** Representative growth curves of *spoT*^{H414A}
536 and *spoT*^{wt} strains containing either the empty vector (EV) or a *gadE* gene on pCA24N or pNTR-SD
537 vectors in M9Glc medium. Two biological replicates each with two technical replicates were
538 performed and presented. **(d)** Normalized percentage of surviving cells of *spoT*^{wt} and *spoT*^{H414A}
539 strains after challenged with media of various pH values. The data were normalized to the starting
540 CFUs of each respective tested strain. **(e)** Heatmap of genes involved in acid resistance. Colored
541 bars indicate genes belonging to the same acid resistance systems: orange, *nuo* genes encoding
542 NADH dehydrogenase I; yellow, *cyo* genes encoding cytochrome *bo* oxidase; green, lysine
543 dependent acid resistance systems; cyan, ornithine dependent acid resistance system; black, alkaline
544 stress; dark blue, arginine dependent acid resistance system.

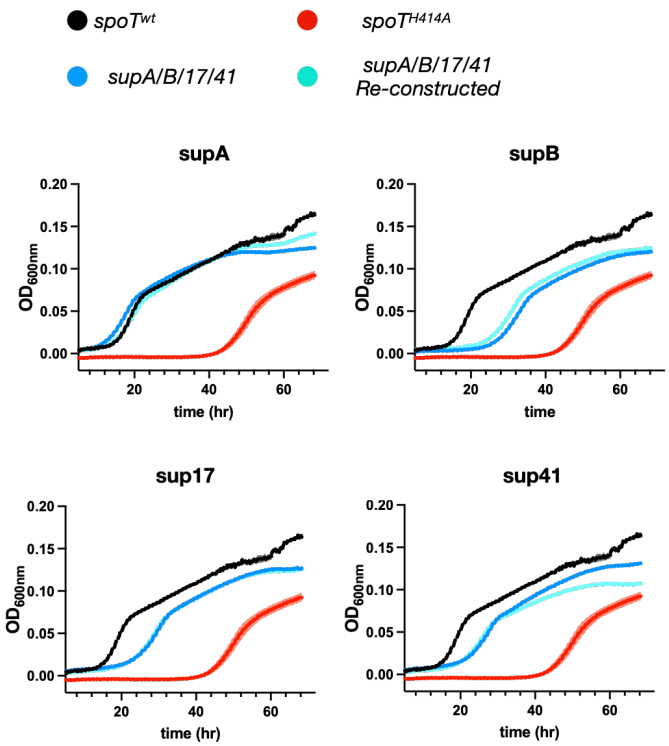

545

546 **Extended Data Fig. 5** Growth dynamics of re-constructed four suppressors (cyan)

547 (*supA/supB/sup17/sup41*) in comparison to *spoT*^{H414A}, *spoT*^{wt}, and the four random suppressors

548 (blue).

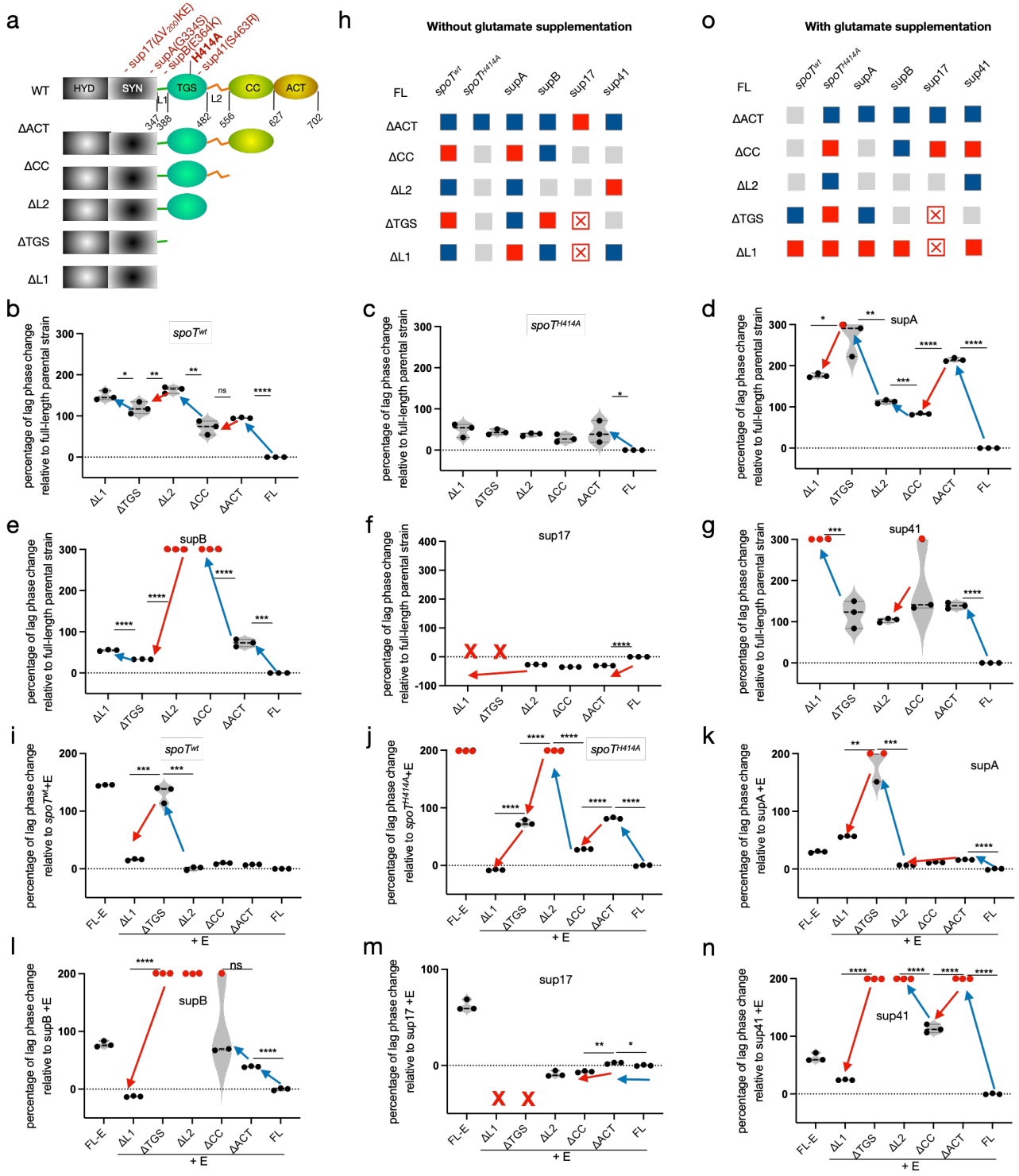

549

550 **Extended Data Fig. 6 (a)** Schematic show of sequential domain truncations of the *spoT* alleles in

551 various strains. **(b-g)** Normalized lag phase length (in percentage) relative to the respective *spoT*-

552 full-length (FL) parental strains during growth in M9Glc. Red dots indicate that the respective

553 strains did not grow up in M9Glc within the tested time frame of 72 hrs. Red crosses indicate the
554 strains could not be made. **(h)** Sum-up of the effect of domain deletions on cell regrowth thus
555 potential regulation of SpoT activity from panels **b-g**. Blue and red blocks indicate positive and
556 negative effects respectively. Red crosses indicate strains impossible to obtain. Grey blocks indicate
557 no effect can be deduced due to insignificant/indistinguishable growth curves. **(i-n)** Normalized lag
558 phase length (in percentage) relative to the respective *spoT*-full-length (FL) parental strains during
559 growth in M9Glc and supplemented with glutamate (0.6 mM). **(o)** Sum-up of the effect of domain
560 deletions on cell regrowth in the presence of supplemented glutamate (0.6 mM) thus potential
561 regulation of SpoT activity from panels **i-n**. Color coding is same as panel **h**.

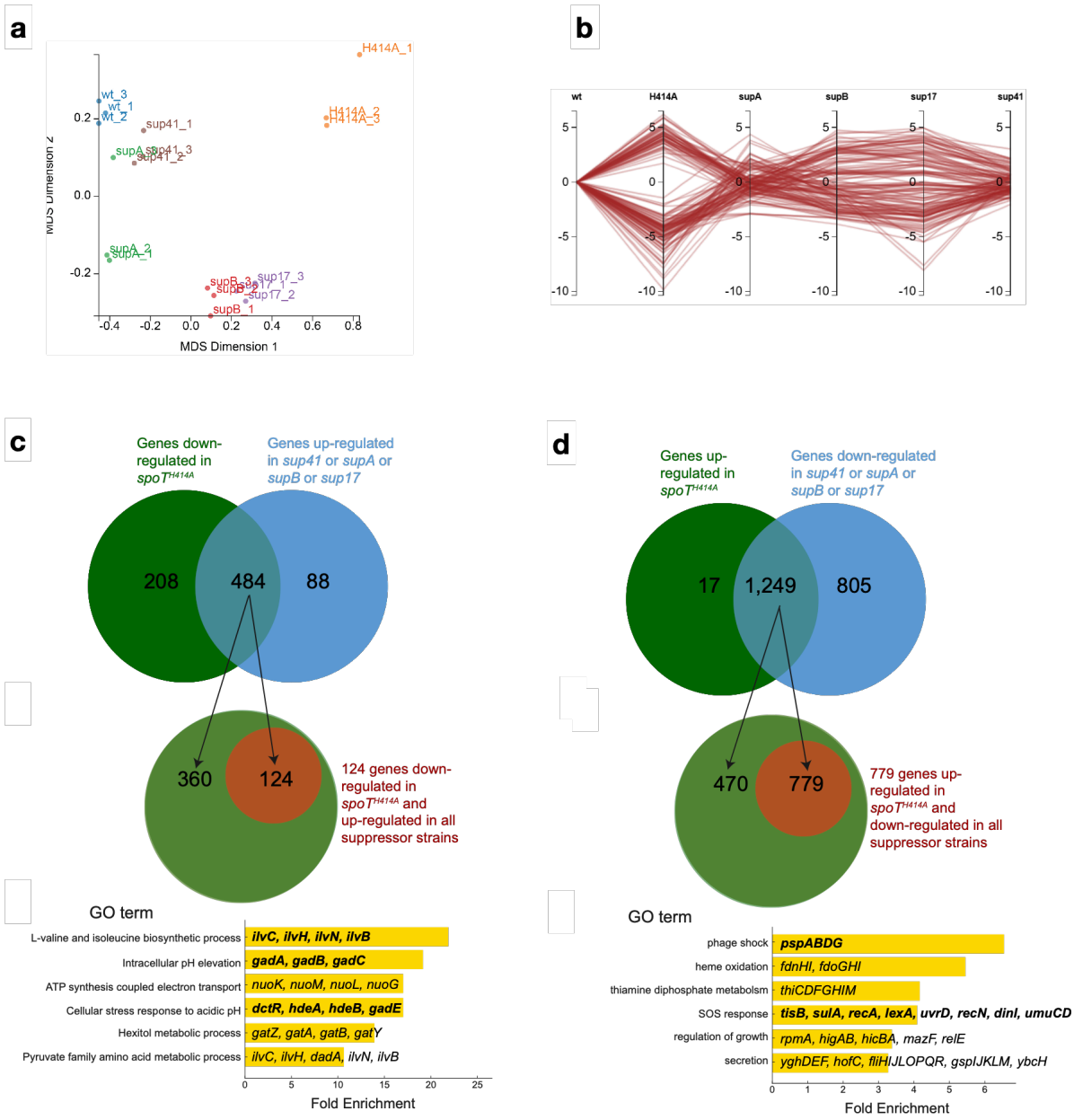

Extended Data Fig. 7 (a) Parallel Coordinates plot of the *spoT*^{wt}, *spoT*^{H414A} and the four suppressor strains with |Log2(FC)| > 4 and FDR < 0.05. (**b**) MDS plot of the six strains showing individual samples. Cell growth and sampling are described in Materials and Methods. Panels **a** and **b** were both generated by DEGUST. **(c)** (Top) Venn diagram of genes downregulated in the *spotT*^{H414A} strain and upregulated in either of the four suppressor strains. (middle) Genes downregulated in the *spotT*^{H414A} strain and upregulated in all four suppressor strains. (bottom) Gene Ontology analysis of the 124 genes downregulated in the *spotT*^{H414A} strain and upregulated in all four suppressor strains.

All genes are listed in **Table S4. (d)** (Top) Venn diagram of genes upregulated in the *spotT*^{H414A} strain and downregulated in either of the four suppressor strains**.** (middle) Genes upregulated in the *spotT*^{H414A} strain and downregulated in all four suppressor strains**.** (bottom) Gene Ontology analysis of the 779 genes upregulated in the *spotT*^{H414A} strain and downregulated in all four suppressor strains. All genes are listed in **Table S4.** Genes were extracted from DEGUST using settings of |Log2(FC)| > 1 and FDR < 0.05. Gene names in bold in GO term are strongly up or downregulated.

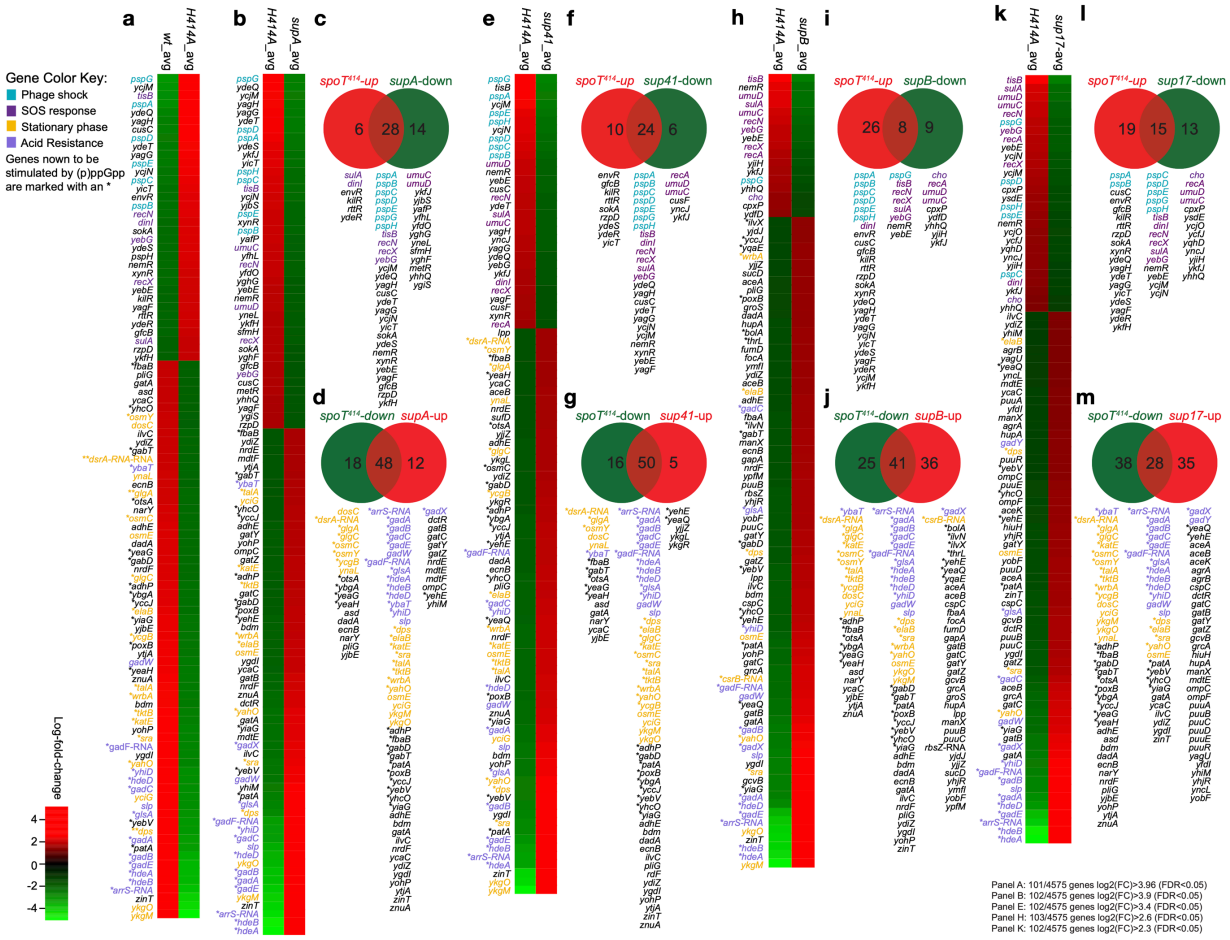

Extended Data Fig. 8 (a) Heatmap of *spoT*^{H414A} versus *spoT*^{wt} (a setting of |Log2(FC)| > 3.96 and FDR < 0.05 returned 100 of a total of 4,575 genes analyzed in DEGUST). Highlighted genes represent phage shock proteins (*psp*, blue), SOS response genes (magenta), acid stress response genes (deep purple), and stationary-phase-induced genes (gold). Genes marked with an asterisk (*)

581 are known ppGpp-inducible genes. (**b, e, h, k)** Heatmaps of *spoT*^{H414A} versus the suppressor strains.
582 FDR settings were identical to those used in (**a**) while the |Log2(FC)| values were set to yield
583 approximately 100 genes to be returned. DEGUST returned 102 genes for *supA* (|Log2(FC)| > 3.9),
584 97 for *sup41* (|Log2(FC)| > 3.4), 94 for *supB* (|Log2(FC)| > 2.6) and 91 for *sup17* (|Log2(FC)|>2.3).
585 The actual genes returned by DEGUST are listed in **Table S5**. **(c, d, f, g, i, j, l, m)** Venn diagram
586 analysis of genes dysregulated in *spoT*^{H414A} and the four suppressor strains. Panel **a** yielded the
587 genes up- and down- regulated in *spoT*^{H414A} relative to the *spoT*^{wt} strain and these genes were used
588 throughout the Venn diagram analysis.

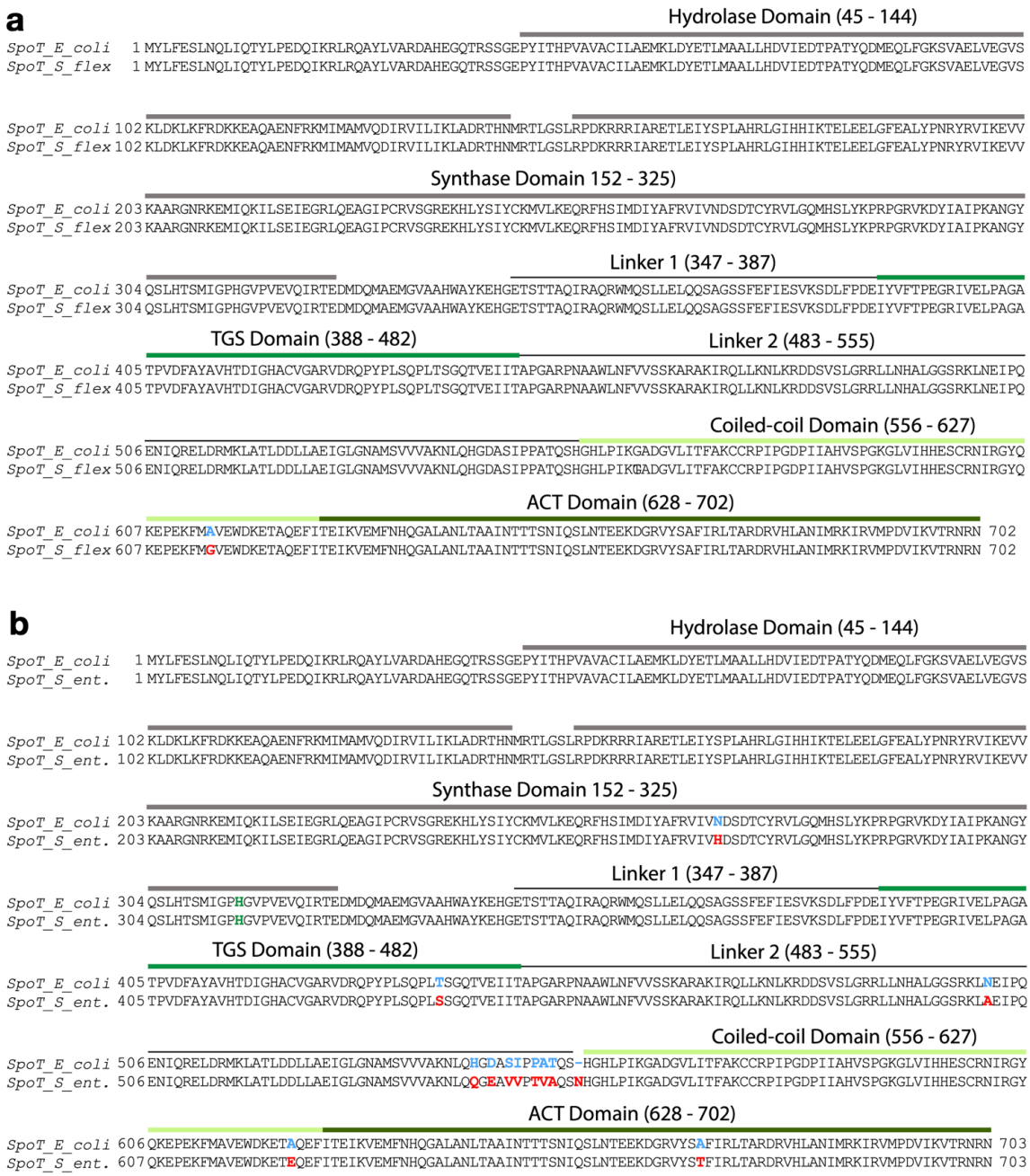

Extended Data Fig. 9 Pairwise sequence comparison between *E. coli* SpoT$_{ec}$ and SpoT from *S. typhimurium* SL1334 and *Shigella flexneri*. *Shigella flexneri* SpoT$_{sf}$ is nearly identical as *E. coli* SpoT$_{ec}$ except for a conserved mutation of Alanine 614 to Glycine on the CC domain. *S. typhimurium* SL1334 SpoT$_{st}$ (702 aa) shares 98.15% identity with *E. coli* SpoT$_{ec}$ (701 aa), with several amino acid variations on the HYD (N267H), TGS (T437S), L2 (nine mutations, N501A,

595 H542Q, D544E, S546V, I547V, P549T, A550V, T551A, an insertion of N between 553-554), CC

596 (A621E), and ACT (A668T) domains.

ACKNOWLEDGEMENTS

We thank Paulina Grucella for helping with Western blot. The work is supported by a Novo Nordisk Foundation Project Grant (NNF19OC0058331), a Danmarks Frie Forskningsfond grant (2032-00030B) to Y.E.Z, the European Union's Horizon 2020 research and innovation programme under the Marie Skłodowska-Curie grant agreement (Nº 801199) to M.L.S, and the Chinese Scholarship Council program (Nº 202206870009) to Y.Y.L.

AUTHOR CONTRIBUTIONS

Y.E.Z designed this study; Y.Y.L, M.L.S and Y.E.Z acquired fundings; Y.Y.L, M.L.S, Y.E.Z acquired experimental data; X.C.Z, L.D, K.G, Y.E.Z performed the bioinformatics analyses; Y.E.Z, K.G, wrote the draft manuscript; and all authors analysed the data and edited the manuscript.

DECLARATIONS OF INTERESTS

The authors declare that they have no conflicts of interest.

EXPERIMENTAL MODEL AND SUBJECT DETAILS

E. coli DH5α (Stratagene) was used for cloning and *E. coli* K-12 MG1655 for experiments requiring an *E. coli* wt strain background (see **Table S1** for further details). For cloning, nutrient broth (Oxoid), with agar and antibiotics (chloramphenicol (25 µg/ml), ampicillin (100 µg/ml), and/or kanamycin (25 µg/ml)) when appropriate, was used. The different MG1655 strains were cultivated in Lysogeny Broth (LB) as well as M9Glc media (1x M9 salt, pH 7.4 1 mM MgSO4, 0.1 mM $CaCl_2$, Thiamine (0.001 mg/1 ml), 0.2 % (g/ml) glucose) at 37 °C with agitation (160 rpm).

METHOD DETAILS

Isolation of suppressor mutations rescuing the growth of *spoT*^{H414A} in M9Glc

621 The *spoT*^{H414A} (YZ527) strain was grown overnight in LB media and then washed twice with PBS
622 buffer. Approx. 10^7 cells were plated on one M9Glc plate and incubated at 30°C. Colonies of different
623 sizes were selected between 24 – 72 hours of incubation, and the restored growth was confirmed in
624 solid and liquid M9Glc medium.
625
626 **Growth assay in liquid minimal media**
627 To measure the growth curves of various strains in M9Glc media, the OD_{600nm} was measured of
628 overnight cultures grown in LB of each strain, washed twice with 1x Phosphate Buffered Saline (PBS)
629 and normalised in PBS and inoculated into fresh M9Glc media with a starting OD_{600nm} = 0.05 unless
630 otherwise stated. The growth was measured every 15 min for 72 hrs in a plate reader (BioTek)
631 presetted at 30°C with double orbital agitation at 548 cpm.
632
633 **Measurements of (p)ppGpp by autoradiography**
634 (p)ppGpp is a highly labile molecule not amenable to HPLC or mass spectrometry analysis. Therefore,
635 thin layer chromatography (TLC) was used to quantify both pppGpp and ppGpp. The excess
636 phosphates in M9Glc affect efficient labelling of nucleotides by $H_3{}^{32}PO_4$, therefore MOPS-M9Glc
637 hybrid media was prepared wherein the PBS buffer in M9Glc was replaced by the MOPS buffer of
638 the MOPS media[43] (i.e., containing MOPS-tricine 40 mM pH 7.2, 1 mM MgSO4, 0.1 mM CaCl2,
639 Thiamine (0.001 mg/1 ml), 0.2 % (g/ml) glucose, NH_4Cl 0.001 g/ml, 8.5 mM NaCl, 0.2 mM $KHPO_4$).
640 The strains were grown for ca. 18 hrs in MOPS-M9Glc media at 37 °C with agitation. Afterwards,
641 the strains were adjusted to the OD_{600nm} of 0.05 in MOPS-M9Glc and grown at 37 °C with agitation
642 until OD_{600nm} of 0.2-0.3 was reached. Then, 100 µl cells were transferred to a 2-ml Eppendorf tube
643 together with 5 µl of 0.005 mCi $H_3{}^{32}PO_4$ (100 µCi/ml, PerkinElmer). After 1h at 37 °C with 600 rpm

644 agitation, 90 µl were transferred to a new tube with 20 µl 2N formic acid, and the sample was stored
645 at -20°C until analysed by TLC as described in[18].
646
647 **Sample preparation for RNA-sequencing**
648 The strains were grown overnight in LB media before washed twice in PBS and inoculated into
649 M9Glc media (OD_{600nm} = 0.05). The strains were grown in M9Glc media until the early exponential
650 phase (approximately OD_{600nm} = 0.2) before the cells were collected, and snap frozen with liquid
651 nitrogen and stored at -80 °C. As the strain *spoT*^{H414A} is unable to grow in M9Glc media, the starting
652 OD_{600nm} was set to 0.2, and the cells were collected when the other strains are ready to harvest, i.e.
653 ca. 18 hrs.
654 Total RNA was extracted using the RNeasy Mini Kit (Qiagen; 74104). Ribosomal RNA (rRNA) was
655 depleted from purified total RNA with Ribo-Zero Plus rRNA Depletion kit (Illumina; 20040892).
656 First and second strand complementary DNA (cDNA) were synthesized by cDNA Synthesis kit
657 (Illumina; 20040895). RNA Index Anchors (Illumina; 20040899) was used for ligation of pre-index
658 anchors to the ends of the double-stranded cDNA fragments to enable dual indexing. Barcoded cDNA
659 libraries were constructed from anchor-ligated DNA fragments and sequenced on Illumina NovaSeq
660 6000 Sequencing System from Genewiz (Azenta Life Sciences), yielding a median depth of
661 39,619,482 paired-end 150 bp reads per sample.
662 **Strain construction**
663 All strains and oligonucleotides used in this study are listed in **Tables S1** and **S2**, respectively. All
664 chromosomal *in situ* mutations of *spoT* alleles were made by using the I-SceI-based λ -Red
665 recombineering method[44].
666
667 <u>The *spoT* E319Q and H72A D73A mutant strains</u>

668 Briefly, the pWRG99 plasmid was transformed into the target strains (YZ38, YZ359, YZ543, YZ544,
669 YZ545, YZ546) creating the target strains YZ313, YZ345, YZ826, YZ827, YZ828, and YZ829. The
670 SceI site of the pWRG100 vector was PCR amplified using the primers pYZ611 and pYZ612 for the
671 E319Q mutation and the primers pYZ617 and pYZ618 for the H72A D73A mutation. These PCR
672 DNAs were then electroporated into the above strains (YZ38, YZ359, YZ543, YZ544, YZ545,
673 YZ546). Then, the oligos pYZ613 and pYZ616 were used to introduce the E319Q and H72A D73A
674 mutations into the specific *spoT* alleles *in situ*, generating the E319Q mutant strains (YZ872, YZ873,
675 YZ874, YZ875, YZ876) and H72A D73A mutant strains (YZ900, YZ902, YZ904, YZ905).
676
677 The C-terminal serial truncated mutant strains of *spoT*
678 pYZ796 and pYZ797 were used to amplify the SceI from pWRG100 and introduced into YZ313,
679 YZ345, YZ826, YZ827, YZ828, and YZ829. The serial truncations were performed using the
680 repairing oligos pYZ798, pYZ799, pYZ901, pYZ801, pYZ902, deleting the according domains
681 (ACT, ACT-CC, ACT-CC-Linker2, ACT-CC-Linker2-TGS, ACT-CC-Linker2-TGS-Linker1,
682 respectively).
683
684 Reconstruction of the $spoT^{H414A}$ suppressor mutations
685 Primers pYZ619 and pYZ620 were used to amplify the SceI DNA from pWRG100 vector before it
686 was introduced into the strain $spoT^{wt}$ (YZ313). Then, the primers pYZ328 and pYZ70 were used to
687 amplify the corresponding *spoT* alleles using the chromosomal DNA of the strains supA (YZ543),
688 *supB* (YZ544), sup17 (YZ545), and sup41 (YZ546) respectively as the templates. These DNAs were
689 used to introduce the specific *spoT* suppressing mutations.
690
691 P1 phage transduction

692 The *spoT* genes of the suppressor strains YZ543, YZ544, YZ545, and YZ546 were inactivated via
693 P1 phage transduction. The donor strain for making the P1 phage lysate was the *spoT207::cat* strain
694 (YZ47)[17], which contains a chloramphenicol resistance cassette together with *spoT207* deletion allele
695 for selection. The phage lysate was used to infect strains YZ543, YZ544, YZ545, and YZ546 and the
696 chloramphenicol resistant transductants were selected and confirmed via diagnostic PCR.
697
698 **Plasmids constructions**
699 To construct *E. coli (Ec), Salmonella typhimurium(st) or Shigella flexneri(sf) spoT* wild type (wt) and
700 H414A mutant plasmids, standard molecular cloning procedures were used. For *E. coli*, the *spoT*
701 coding sequence was PCR-amplified from MG1655 $spoT^{wt}$ (YZ38) or $spoT^{H414A}$ (YZ527) using
702 primers pYZ1201 and pYZ1202. The pBAD33 vector was isolated from *E. coli* DH5α (YZ593). Both
703 the amplified *spoT* fragments and pBAD33 were digested with *KpnI* and *HindIII* and ligated using
704 T4 DNA ligase to generate pBAD33- $spoT^{wt}$ and pBAD33- $spoT^{H414A}$. For *S. Typhimurium*, the
705 H414A mutation was introduced into pGEN-MCS-$spoT_{St}$ (YZ692)[45] by site-directed mutagenesis
706 using primers pYZ1312 and pYZ1313, yielding pGEN-MCS-$spoT_{st}$ (H414A). For *S. flexneri*, an
707 A614G substitution was introduced by overlap-extension PCR using pBAD33-$spoT_{Ec}$(wt) or
708 pBAD33- $spoT_{Ec}$(H414A) as templates. Upstream and downstream fragments were amplified with
709 primer pairs pYZ1201/pYZ1346 and pYZ1202/pYZ1345, respectively, fused by overlap PCR using
710 primers pYZ1201 and pYZ1202, and cloned into pBAD33 following digestion with *KpnI* and *HindIII*
711 to generate pBAD33-$spoT_{Sf}$(WT) and pBAD33-$spoT_{Sf}$(H414A). To construct the plasmid pCA24N-
712 argA(H15Y), quick-change mutagenesis was carried out using pCA24N-argA(wt) as template and
713 the primers pYZ1168 and pYZ1169. All plasmids were transformed into *E. coli* DH5α (see **Table**
714 **S1**), purified using a commercial miniprep kit (NEB-T1110L), and confirmed by sequencing with

715 primers pYZ404, pYZ405, and pYZ71 (for pBAD33 constructs), pYZ1305, pYZ1306, and pYZ1228
716 (for pGEN-MCS constructs) or pYZ34 and pYZ35 (for pCA24N constructs; Eurofins Genomics).

717

718 **Acid resistance assay**

719 Overnight (16 hrs) cultures were grown in LB medium at 37°C with shaking (160 rpm). Cells were
720 harvested by centrifugation, washed twice with PBS, and normalized to an optical density at 600 nm
721 (OD_{600nm}) of 0.4 in minimal medium supplemented with 0.2% glucose (M9Glc, pH 7.4). Cultures
722 were incubated at 37°C with shaking (160 rpm) for 30 min to allow adaptation to M9Glc. After
723 adaptation, 1 mL cells were pelleted and resuspended in the same volume of M9Glc medium pre-
724 adjusted to various pH values (from 2.5 to 8.0), with or without supplemented 0.6 mM glutamate (or
725 other amino acids). Acid challenge was then performed and assessed at 37°C with shaking (160 rpm).
726 Cell viability was determined at time zero (i.e., before shifting to M9Glc with a low pH), and at 0.5,
727 1, 2 and 4 h after acid challenges. For viable-cell counts, 40 μL cell culture at each time point was
728 collected and 10-fold serially diluted (10^0–10^{-7}) in LB medium, and 5 μL of each dilution was spotted
729 on LB agar plates, allowing colony formation and enumeration and calculation of CFUs the next day.

730

731 **Western blot**

732 Western blot analysis of protein levels of various mutant SpoT was performed as reported[46]. Briefly,
733 cells of various strains were collected the same manner as preparation for RNA sequencing (see above,
734 and **Fig. S1C**). These cells were normalised to have an equal OD_{600nm} per ml and mixed with 2x SDS-
735 PAGE loading buffer. Samples were heated for 15 min at 95°C and 20 ul of each were separated in
736 10% SDS-PAGE gels. The proteins were transferred to a PVDF membrane (Amersham) and the SpoT
737 proteins detected by first incubation with anti-SpoT antiserum (Covalab) and then the secondary HRP

conjugated rabbit IgG antibody (SIGMA). The SpoT bands were visualized by using the Pierce ECL chemiluminescence substrate (Thermo) and the signals were detected by an Imagequant LAS4100.

Bioinformatic analysis

Preparing RNA-seq data. RNA-seq data (fastq files) were mapped by the BWA-MEM tool of Galaxy [47] and then analysed by the featureCounts tool in Galaxy https://usegalaxy.eu/). The tabular format of the featureCounts files were exported from Galaxy and assembled into one single tabular file from which sub-files containing collections of genes of interest, e.g. amino acid biosynthesis, purine de novo synthesis, were extracted.

Analysis of RNA-seq data. To generate heatmaps and fold-of-changes, the tabular files containing the RNA-seq counts were analysed by DEGUST (https://degust.erc.monash.edu/). To generate Venn diagrams, gene lists were analysed by the jVenn application at (https://jvenn.toulouse.inrae.fr/app/index.html). Gene Ontology terms were generated by AmiGO (https://amigo.geneontology.org/amigo) and Panther (https://pantherdb.org/webservices/go/overrep.jsp). The json-files generated by PANTHER were analysed by ChatGPT that generated editable SVG files.

Other Bioinformatic Procedures

Protein sequence alignment was accomplished using JalView[48], protein tertiary structure modelling and visualization by AlphaFold 3 and ChimeraX, respectively[49,50].

QUANTIFICATION AND STATISTICAL ANALYSIS

761 Signals of (p)ppGpp from autoradiography were quantified using ImageQuant (GE Healthcare). At
762 least three biological replicates were performed and one representative shown in the **Figure**s.
763 For other physiological growth experiments, at least two biological replicates each with three
764 technical replicates were done (see **Figure** legends for details). The length (hours) of lag phases was
765 defined as the period from the growth start to the time point where the slope of growth curves first
766 reaches the exponential-phase growth rate. These lag phage length values were then normalized to
767 the parental strains or conditions, and plotted (see each of the legends for details). The student *t*-test
768 was used for statistic analysis wherever applicable.
769

770 **DATA AVAILABILITY**

771 The RNA-seq raw data produced in this study are available through the NCBI Sequence Read
772 Archive under BioProject accession number PRJNA1097790.

References

1. Fang, F.C., Frawley, E.R., Tapscott, T., and Vázquez-Torres, A. (2016). Bacterial Stress Responses during Host Infection. Cell Host Microbe *20*, 133-143. 10.1016/j.chom.2016.07.009.
2. Lin, J., Smith, M.P., Chapin, K.C., Baik, H.S., Bennett, G.N., and Foster, J.W. (1996). Mechanisms of acid resistance in enterohemorrhagic Escherichia coli. Appl Environ Microbiol *62*, 3094-3100. 10.1128/aem.62.9.3094-3100.1996.
3. Kanjee, U., and Houry, W.A. (2013). Mechanisms of acid resistance in Escherichia coli. Annu Rev Microbiol *67*, 65-81. 10.1146/annurev-micro-092412-155708.
4. Lund, P., Tramonti, A., and De Biase, D. (2014). Coping with low pH: molecular strategies in neutralophilic bacteria. FEMS Microbiol Rev *38*, 1091-1125. 10.1111/1574-6976.12076.
5. Capitani, G., De Biase, D., Aurizi, C., Gut, H., Bossa, F., and Grütter, M.G. (2003). Crystal structure and functional analysis of Escherichia coli glutamate decarboxylase. Embo j *22*, 4027-4037. 10.1093/emboj/cdg403.
6. Castanie-Cornet, M.P., Penfound, T.A., Smith, D., Elliott, J.F., and Foster, J.W. (1999). Control of acid resistance in Escherichia coli. J Bacteriol *181*, 3525-3535. 10.1128/jb.181.11.3525-3535.1999.
7. Irving, S.E., Choudhury, N.R., and Corrigan, R.M. (2021). The stringent response and physiological roles of (pp)pGpp in bacteria. Nat Rev Microbiol *19*, 256-271. 10.1038/s41579-020-00470-y.
8. Anderson, B.W., Fung, D.K., and Wang, J.D. (2021). Regulatory Themes and Variations by the Stress-Signaling Nucleotide Alarmones (p)ppGpp in Bacteria. Annu Rev Genet *55*, 115-133. 10.1146/annurev-genet-021821-025827.
9. Bange, G., Brodersen, D.E., Liuzzi, A., and Steinchen, W. (2021). Two P or Not Two P: Understanding Regulation by the Bacterial Second Messengers (p)ppGpp. Annu Rev Microbiol *75*, 383-406. 10.1146/annurev-micro-042621-122343.
10. Hauryliuk, V., Atkinson, G.C., Murakami, K.S., Tenson, T., and Gerdes, K. (2015). Recent functional insights into the role of (p)ppGpp in bacterial physiology. Nat Rev Microbiol *13*, 298-309. 10.1038/nrmicro3448.
11. Block, R., and Haseltine, A.W. (1975). Purification and properties of stringent factor. J Biol Chem *250*, 1212-1217.
12. Brown, A., Fernández, I.S., Gordiyenko, Y., and Ramakrishnan, V. (2016). Ribosome-dependent activation of stringent control. Nature *534*, 277-280. 10.1038/nature17675.
13. Loveland, A.B., Bah, E., Madireddy, R., Zhang, Y., Brilot, A.F., Grigorieff, N., and Korostelev, A.A. (2016). Ribosome•RelA structures reveal the mechanism of stringent response activation. Elife *5*. 10.7554/eLife.17029.
14. Arenz, S., Abdelshahid, M., Sohmen, D., Payoe, R., Starosta, A.L., Berninghausen, O., Hauryliuk, V., Beckmann, R., and Wilson, D.N. (2016). The stringent factor RelA adopts an open conformation on the ribosome to stimulate ppGpp synthesis. Nucleic Acids Res *44*, 6471-6481. 10.1093/nar/gkw470.
15. Winther, K.S., Roghanian, M., and Gerdes, K. (2018). Activation of the Stringent Response by Loading of RelA-tRNA Complexes at the Ribosomal A-Site. Mol Cell *70*, 95-105.e104. 10.1016/j.molcel.2018.02.033.

817 16. Ross, W., Vrentas, C.E., Sanchez-Vazquez, P., Gaal, T., and Gourse, R.L. (2013). The magic
818 spot: a ppGpp binding site on E. coli RNA polymerase responsible for regulation of
819 transcription initiation. Mol Cell *50*, 420-429. 10.1016/j.molcel.2013.03.021.
820 17. Ross, W., Sanchez-Vazquez, P., Chen, A.Y., Lee, J.H., Burgos, H.L., and Gourse, R.L. (2016).
821 ppGpp Binding to a Site at the RNAP-DksA Interface Accounts for Its Dramatic Effects on
822 Transcription Initiation during the Stringent Response. Mol Cell *62*, 811-823.
823 10.1016/j.molcel.2016.04.029.
824 18. Zhang, Y.E., Bærentsen, R.L., Fuhrer, T., Sauer, U., Gerdes, K., and Brodersen, D.E. (2019).
825 (p)ppGpp Regulates a Bacterial Nucleosidase by an Allosteric Two-Domain Switch. Mol Cell
826 *74*, 1239-1249.e1234. 10.1016/j.molcel.2019.03.035.
827 19. Zhang, Y., Zborníková, E., Rejman, D., and Gerdes, K. (2018). Novel (p)ppGpp Binding and
828 Metabolizing Proteins of Escherichia coli. mBio *9*. 10.1128/mBio.02188-17.
829 20. Wang, B., Grant, R.A., and Laub, M.T. (2020). ppGpp Coordinates Nucleotide and Amino-
830 Acid Synthesis in E. coli During Starvation. Mol Cell *80*, 29-42.e10.
831 10.1016/j.molcel.2020.08.005.
832 21. Wang, B., Dai, P., Ding, D., Del Rosario, A., Grant, R.A., Pentelute, B.L., and Laub, M.T.
833 (2019). Affinity-based capture and identification of protein effectors of the growth regulator
834 ppGpp. Nat Chem Biol *15*, 141-150. 10.1038/s41589-018-0183-4.
835 22. Sanchez-Vazquez, P., Dewey, C.N., Kitten, N., Ross, W., and Gourse, R.L. (2019). Genome-
836 wide effects on Escherichia coli transcription from ppGpp binding to its two sites on RNA
837 polymerase. Proc Natl Acad Sci U S A *116*, 8310-8319. 10.1073/pnas.1819682116.
838 23. Traxler, M.F., Summers, S.M., Nguyen, H.T., Zacharia, V.M., Hightower, G.A., Smith, J.T.,
839 and Conway, T. (2008). The global, ppGpp-mediated stringent response to amino acid
840 starvation in Escherichia coli. Mol Microbiol *68*, 1128-1148. 10.1111/j.1365-
841 2958.2008.06229.x.
842 24. Durfee, T., Hansen, A.M., Zhi, H., Blattner, F.R., and Jin, D.J. (2008). Transcription profiling
843 of the stringent response in Escherichia coli. J Bacteriol *190*, 1084-1096. 10.1128/jb.01092-
844 07.
845 25. Grucela, P.K., Fuhrer, T., Sauer, U., Chao, Y., and Zhang, Y.E. (2023). Ribose 5-phosphate:
846 the key metabolite bridging the metabolisms of nucleotides and amino acids during stringent
847 response in Escherichia coli? Microb Cell *10*, 141-144. 10.15698/mic2023.07.799.
848 26. Haseltine, W.A., and Block, R. (1973). Synthesis of guanosine tetra- and pentaphosphate
849 requires the presence of a codon-specific, uncharged transfer ribonucleic acid in the acceptor
850 site of ribosomes. Proc Natl Acad Sci U S A *70*, 1564-1568. 10.1073/pnas.70.5.1564.
851 27. Xiao, H., Kalman, M., Ikehara, K., Zemel, S., Glaser, G., and Cashel, M. (1991). Residual
852 guanosine 3',5'-bispyrophosphate synthetic activity of relA null mutants can be eliminated by
853 spoT null mutations. J Biol Chem *266*, 5980-5990.
854 28. Fernández-Coll, L., and Cashel, M. (2020). Possible Roles for Basal Levels of (p)ppGpp:
855 Growth Efficiency Vs. Surviving Stress. Front Microbiol *11*, 592718.
856 10.3389/fmicb.2020.592718.
857 29. Seyfzadeh, M., Keener, J., and Nomura, M. (1993). spoT-dependent accumulation of
858 guanosine tetraphosphate in response to fatty acid starvation in Escherichia coli. Proc Natl
859 Acad Sci U S A *90*, 11004-11008. 10.1073/pnas.90.23.11004.
860 30. Battesti, A., and Bouveret, E. (2006). Acyl carrier protein/SpoT interaction, the switch linking
861 SpoT-dependent stress response to fatty acid metabolism. Mol Microbiol *62*, 1048-1063.
862 10.1111/j.1365-2958.2006.05442.x.

863 31. Vinella, D., Albrecht, C., Cashel, M., and D'Ari, R. (2005). Iron limitation induces SpoT-
864 dependent accumulation of ppGpp in Escherichia coli. Mol Microbiol *56*, 958-970.
865 10.1111/j.1365-2958.2005.04601.x.
866 32. Spira, B., Silberstein, N., and Yagil, E. (1995). Guanosine 3',5'-bispyrophosphate (ppGpp)
867 synthesis in cells of Escherichia coli starved for Pi. J Bacteriol *177*, 4053-4058.
868 10.1128/jb.177.14.4053-4058.1995.
869 33. Dalebroux, Z.D., Svensson, S.L., Gaynor, E.C., and Swanson, M.S. (2010). ppGpp conjures
870 bacterial virulence. Microbiol Mol Biol Rev *74*, 171-199. 10.1128/mmbr.00046-09.
871 34. Levin-Reisman, I., Ronin, I., Gefen, O., Braniss, I., Shoresh, N., and Balaban, N.Q. (2017).
872 Antibiotic tolerance facilitates the evolution of resistance. Science *355*, 826-830.
873 10.1126/science.aaj2191.
874 35. Windels, E.M., Michiels, J.E., Fauvart, M., Wenseleers, T., Van den Bergh, B., and Michiels,
875 J. (2019). Bacterial persistence promotes the evolution of antibiotic resistance by increasing
876 survival and mutation rates. Isme j *13*, 1239-1251. 10.1038/s41396-019-0344-9.
877 36. Lewis, K. (2007). Persister cells, dormancy and infectious disease. Nat Rev Microbiol *5*, 48-
878 56. 10.1038/nrmicro1557.
879 37. Harms, A., Maisonneuve, E., and Gerdes, K. (2016). Mechanisms of bacterial persistence
880 during stress and antibiotic exposure. Science *354*. 10.1126/science.aaf4268.
881 38. Rajagopal, B.S., DePonte, J., 3rd, Tuchman, M., and Malamy, M.H. (1998). Use of inducible
882 feedback-resistant N-acetylglutamate synthetase (argA) genes for enhanced arginine
883 biosynthesis by genetically engineered Escherichia coli K-12 strains. Appl Environ Microbiol
884 *64*, 1805-1811. 10.1128/aem.64.5.1805-1811.1998.
885 39. Zhou, Y.N., and Jin, D.J. (1998). The rpoB mutants destabilizing initiation complexes at
886 stringently controlled promoters behave like "stringent" RNA polymerases in Escherichia coli.
887 Proc Natl Acad Sci U S A *95*, 2908-2913. 10.1073/pnas.95.6.2908.
888 40. Zhang, Y.E., Baerentsen, R.L., Fuhrer, T., Sauer, U., Gerdes, K., and Brodersen, D.E. (2019).
889 (p)ppGpp Regulates a Bacterial Nucleosidase by an Allosteric Two-Domain Switch. Mol Cell
890 *74*, 1239-1249 e1234. 10.1016/j.molcel.2019.03.035.
891 41. Kitagawa, M., Ara, T., Arifuzzaman, M., Ioka-Nakamichi, T., Inamoto, E., Toyonaga, H., and
892 Mori, H. (2005). Complete set of ORF clones of Escherichia coli ASKA library (a complete
893 set of E. coli K-12 ORF archive): unique resources for biological research. DNA Res *12*, 291-
894 299. 10.1093/dnares/dsi012.
895 42. Saka, K., Tadenuma, M., Nakade, S., Tanaka, N., Sugawara, H., Nishikawa, K., Ichiyoshi, N.,
896 Kitagawa, M., Mori, H., Ogasawara, N., and Nishimura, A. (2005). A complete set of
897 Escherichia coli open reading frames in mobile plasmids facilitating genetic studies. DNA
898 Res *12*, 63-68. 10.1093/dnares/12.1.63.
899 43. Neidhardt, F.C., Bloch, P.L., and Smith, D.F. (1974). Culture medium for enterobacteria. J
900 Bacteriol *119*, 736-747. 10.1128/jb.119.3.736-747.1974.
901 44. Kanjee, U., Gutsche, I., Alexopoulos, E., Zhao, B., El Bakkouri, M., Thibault, G., Liu, K.,
902 Ramachandran, S., Snider, J., Pai, E.F., and Houry, W.A. (2011). Linkage between the
903 bacterial acid stress and stringent responses: the structure of the inducible lysine
904 decarboxylase. Embo j *30*, 931-944. 10.1038/emboj.2011.5.
905 45. Chau, N.Y.E., Perez-Morales, D., Elhenawy, W., Bustamante, V.H., Zhang, Y.E., and
906 Coombes, B.K. (2021). (p)ppGpp-Dependent Regulation of the Nucleotide Hydrolase PpnN
907 Confers Complement Resistance in Salmonella enterica Serovar Typhimurium. Infect Immun
908 *89*. 10.1128/IAI.00639-20.

46. Towbin, H., Staehelin, T., and Gordon, J. (1979). Electrophoretic transfer of proteins from polyacrylamide gels to nitrocellulose sheets: procedure and some applications. Proc Natl Acad Sci U S A *76*, 4350-4354. 10.1073/pnas.76.9.4350.
47. The Galaxy platform for accessible, reproducible, and collaborative data analyses: 2024 update. (2024). Nucleic Acids Res *52*, W83-w94. 10.1093/nar/gkae410.
48. Procter, J.B., Carstairs, G.M., Soares, B., Mourão, K., Ofoegbu, T.C., Barton, D., Lui, L., Menard, A., Sherstnev, N., Roldan-Martinez, D., et al. (2021). Alignment of Biological Sequences with Jalview. Methods Mol Biol *2231*, 203-224. 10.1007/978-1-0716-1036-7_13.
49. Senior, A.W., Evans, R., Jumper, J., Kirkpatrick, J., Sifre, L., Green, T., Qin, C., Žídek, A., Nelson, A.W.R., Bridgland, A., et al. (2020). Improved protein structure prediction using potentials from deep learning. Nature *577*, 706-710. 10.1038/s41586-019-1923-7.
50. Pettersen, E.F., Goddard, T.D., Huang, C.C., Meng, E.C., Couch, G.S., Croll, T.I., Morris, J.H., and Ferrin, T.E. (2021). UCSF ChimeraX: Structure visualization for researchers, educators, and developers. Protein Sci *30*, 70-82. 10.1002/pro.3943.

925 **Legends to Supplementary Tables**

926 **Table S1. Bacterial strains used in this study**

927 **Table S2. Oligonucleotides used in this study**

928 **Table S3. Differential gene expression analysis of RNA-seq data from *spoT*^{wt} and *spoT*^{H414A}**

929 **strains .** In total, the transcription levels of 4575 genes of MG1655 were analysed. At a setting of

930 |Log2(FC)| > 1 and FDR < 0.05, 865 and 949 genes were down and up-regulated, respectively. The

931 change-of-folds |Log2(FC)| of each gene are also shown.

932

933 **Table S4. Gene ontology analysis of the four suppressor strains.**

934 **Sheet #1 (related to Extended Data Fig. 7C):** Genes downregulated in the *spoT*^{H414A} strain relative

935 to the *spoT*^{wt} strain (Column A). Genes upregulated in either of the four suppressor strains *supA*,

936 *sup41*, *supB* and *sup17* relative to the *spoT*^{H414A} strain (Columns B to E). The list of genes in

937 Columns B to E were used to generate a list of genes that were upregulated in at least one

938 suppressor strain (Column F) and a list of genes that were upregulated in all 4 suppressor strains

939 (Column G).

940

941 **Sheet #2 (related to Extended Data Fig. 7D):** Genes upregulated in the *spoT*^{H414A} strain relative

942 to the *spoT*^{wt} strain (Column A). Genes downregulated in either of the four suppressor strains

943 relative to the *spoT*^{H414A} strain. The list of genes in Columns B to E were used to generate a list of

944 genes that were upregulated in at least one suppressor strain (Column F) and a list of genes that

945 were downregulated in all 4 suppressor strains (Column G). Gene lists in **Table S4** were generated

946 by DEGUST at a setting of |Log2(FC)| > 1 and FRD < 0.05.

947

948 **Table S5. Comparison of *spoT*^{H414A} with suppressor strains (related to Extended Data Fig. 8).**

949 The Table yields the folds-of-changes in the suppressor strains relative to *spoT*^{H414A}. The Log2(FC)

950 setting in DEGUST was chosen to yield around 100 genes up and downregulated in each heatmap

951 Panels a, b, e, h and k of **Extended Data Fig. 8**.